Rijksuniversiteit Groningen

Bachelor Thesis

Collisional Excitation of Interstellar NH, ND and CH_3OCHO

Author:
N.P. Foley

Supervisor:
F. van der Tak

Abstract

The excitation of molecular species under interstellar conditions is an interplay between collisional and radiative processes. Understanding this balance requires calculations which take both processes into account. However, the required input data are often missing, especially on the collision side. This thesis presents a study into the collisional excitation of the interstellar molecules NH, its isotopologue ND and CH_3OCHO, with the aim of investigating their collisionally-induced spectral features in the environments that they populate, as well as setting constraints on detecting the molecular spectra. Data files that unified both spectroscopic and collision data were compiled and run through the radiative transfer program RADEX. It was found that for NH and ND in diffuse molecular clouds, the produced emission lines are and will most likely remain undetectable, whereas in dark clouds they might be, provided sufficient instrument sensitivity and exposure time, as well as noise being kept to a minimum. CH_3OCHO was found to meet detection requirements in dark clouds. The key implication of the results are that it is now possible to directly infer abundances of the aforementioned interstellar species based on observed spectral features and knowledge about the environments that they inhabit.

Contents

1 Introduction

The interstellar medium, or ISM for short, is comprised of essentially everything that lies between stars, from interstellar gas and dust to cosmic rays. It is arguably one of the most important components of any galaxy, including the Milky Way, because it is within the ISM that star formation occurs. Metaphorically speaking, stars and the ISM are hence the life and blood of a galaxy. Star formation is but one of a plethora of processes that occur in the ISM. Others include shock waves originating from supernovas that make their way through and cause large scale perturbations in interstellar clouds, the acceleration of charged particles to give rise to cosmic rays, but also the formation of interstellar molecules (Maciel, 2015, Draine, 2011).

The study of interstellar abundances, be they atomic or molecular, and reactions is attributed to the field of astrochemistry. The advancements of both observational and experimental spectroscopy have lead to the detection of close to three hundred interstellar molecules in the last 80 years. This thesis will focus on three such molecules, namely the isotopologues NH and ND, where D stands for the hydrogen isotope of molecular mass 2 named deuterium, and methyl formate. In the following, the chemistry of these species and the environments where they can be found will be touched upon as part of the introduction. The section will conclude with the positing of research questions, which serve as paving the way for a closer investigation of not only the aforementioned species themselves , but also of what these species reveal about processes occurring in the ISM regions that they inhabit.

1.1 Chemistry of NH and ND

Interstellar hydrides, which are molecules containing at least one hydrogen atom bonded to one heavier element, were among the first molecules detected beyond our solar system (Gerin et al., 2016). Given that their formation processes are relatively simple and straightforward, they are among the first molecules to form in initially-atomic gas, in addition to molecular hydrogen and hydride-associated ions. Moreover, the abundances of different hydride species yield key insights about the physical and chemical processes of the environment in which they are found and formed (Gerin et al., 2016). This makes them crucial and fundamental players in astrochemistry.

Nitrogen, the seventh element in the periodic table and the fifth most abundant nuclide in the universe (Hily-Blant et al., 2010), figures among the principal heavier atoms present in interstellar hydrides (Gerin et al., 2016). Its high electronegativity (PubChem, n.d.) means that it has a high inclination to form covalent bonds which is an essential aspect when bonding to Hydrogen atoms. There are numerous nitrogen hydride species including ammonia (NH_3), the most common, its protonated form, ammonium, (NH_4^+), the amidogen radical (NH_2) and, most importantly for this project, the imidogen radical (NH). Nitrogen hydrides predominantly form via a series of hydrogen abstraction reactions starting from $N^+ + H_2 \rightarrow NH^+ + H$, a slightly endothermic reaction driven by UV radiation which is more efficient with o-H_2, meaning that the spin of the hydrogen atoms are aligned, than with its spin isomer p-H_2. Subsequent hydrogen abstraction

reactions all follow the same pattern, namely $NH_n^+ + H_2 \rightarrow NH_{n+1}^+ + H$ with n=1,2,3. The neutral hydrides are then formed through dissociative recombination $NH_{n+1}^+ + e^- \rightarrow NH_n + H$ (Gerin et al., 2016). NH, in particular, can also be formed through different mechanisms. In diffuse clouds, a major formation mechanism is $H^- + N \rightarrow NH + e^-$ (Prasad and Huntress, 1980). Additionally, NH is also a secondary product of the dissociative recombination of N_2H^+, with the primary products being N_2+H (Vigren et al., 2012). NH formation through grain catalysis has also been proposed, though there is still much to be investigated to concerning the exact formation mechanisms and the production rate. ND can form in a way that is quite similar to NH, starting from N^+ and HD, the deuterated form of H_2, to form ND^+ and H. Analogously to NH^+, ND^+ can engage in hydrogen abstraction reactions followed by the dissociative recombination of NHD^+ (or NH_2D^+ to form ND). Another ND formation mechanism proposed by Bacmann et al., 2010 starts from proton-deuteron exchange with NH, namely $NH+H_2D^+ \rightarrow NHD^+ + H_2$, followed by the dissociative recombination of NHD^+. NH, along with the other simple nitrogen hydrides, are frequent stepping stones in the formation of more complex nitrogen-bearing molecules (Le Gal et al., 2014). All of the aforementioned species have been detected in the ISM with the discovery of interstellar NH dating back to 1991 (Meyer and Roth, 1991), where its absorption band near 3358 Å was detected in the diffuse clouds toward the stars HD27778 and ζ Per, respectively. NH's deuterated counterpart, ND, was also detected more recently thanks to its far-IR rotational absorption lines at 522.1 and 546.2 GHz in the envelope of the solar-mass protostar IRAS16293-2422 (Bacmann et al., 2010) with the heterodyne instrument HIFI as part of the Herschel key programme known as the Chemical Herschel Survey of Star forming regions, or CHESS for short. ND is rarer than NH, with estimates of the fractional abundance of ND with respect to NH being $30-100\%$ according to Bacmann et al., 2010 with Gerin et al., 2016 putting that figure at around 10%, though with large uncertainties due to the difference in excitation between NH and ND. Deuterated imidogen nonetheless provides relevant astrochemical insights. Its observation, though difficult, allows to better trace the evolution of gas and dust during star formation and sheds light on isotopic fractionation processes conducive to its formation (Melosso et al., 2019).

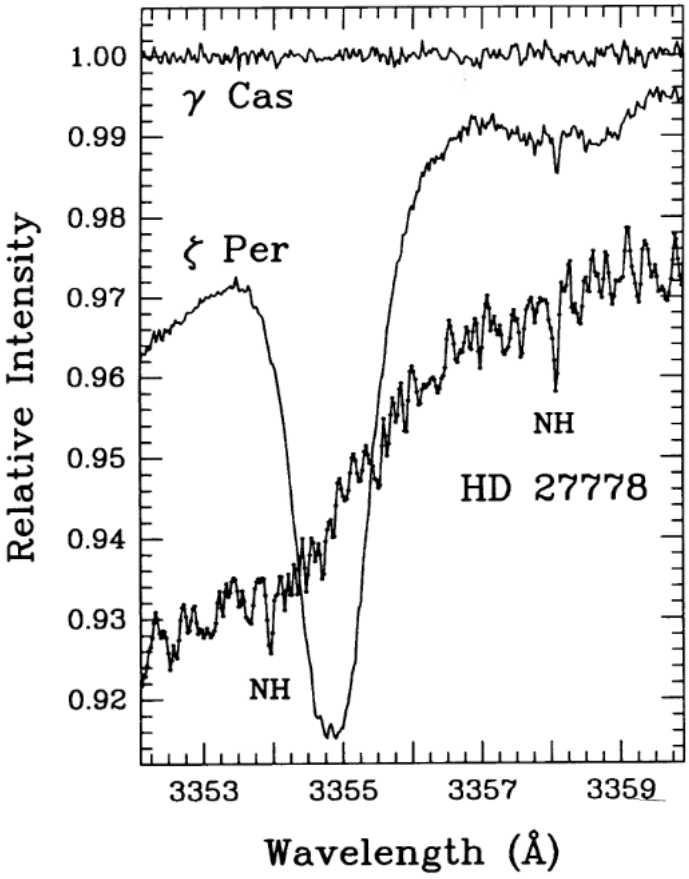

Figure 1: Comparison between the spectra of the clouds ζ Per, HD 27778 and γ Cas in the 3358 Å spectral region of NH as shown in Meyer and Roth, 1991. The spectra are shown at the same relative intensity, albeit for a vertical offset applied to ζ Per and HD 27778. The large absorption line in the ζ Per spectrum around 3355 Å corresponds to a blend of a He I and Ne II line. The NH $A^3\Pi - X^3\Sigma(0,0)R_1(0)$ line at 3358 Å is clearly visible for both ζ Per and HD 27778, but missing for flattend spectrum of γ Cas. HD 27778, additionally, shows the ${}^RQ_{12}(0)$ line at rest wavelength 3354 Å.

Since its first detection, NH has also been observed in various other sources (of the order 10) thanks to the Herschel HIFI instrument (Roueff and Lique, 2013). It is largely agreed that NH is mainly found in diffuse molecular clouds (Gerin et al., 2016) , but also in cold dark clouds (Le Gal et al., 2014), the precursors of stars. Diffuse molecular clouds are regions in the interstellar medium where the interstellar radiation field is sufficiently attenuated such that the fraction of hydrogen in its molecular form becomes significant ($> 10\%$), with column densities of H_2 lying between 10^{20} and 10^{22} cm^{-2} (Snow and McCall, 2006). Diffuse molecular clouds are also, generally speaking, encompassed by atomic clouds which provide shielding from UV radiation which otherwise would dissociate the molecular gas. This entails that any line of

sight crossing a diffuse molecular cloud, will almost inevitably cross an atomic cloud as well. Due to its relatively high abundance in H_2, diffuse molecular clouds provide fertile grounds for chemical reactions to initiate and molecules to form. Typical hydrogen densities of these clouds are estimated to be between 100 and 500 cm^{-3}, whereas its temperature range is said to be 30−100K. Cold dark clouds, on the other hand, are made almost entirely of molecular hydrogen and have kinetic temperatures between 10K to 20K and are far denser than their diffuse counterparts, with densities spanning $10^3 - 10^4$ cm^{-3}, and even 10^5 cm^{-3} in their cores (Bergin and Tafalla, 2007). Due to the high densities, the inner regions of such clouds are extremely well shielded from UV radiation. These clouds are called dark, not because of their molecular hydrogen composition, but because they are also populated by dust grains that absorb optical light and thus dim the starlight emanating from behind such a cloud in our line of sight. The dust is thus heated by the interstellar radiation field, and it emits in the far-IR, which is an important factor to consider due to that NH and ND (and methyl formate) given that they radiate in the sub-millimeter wavelength range. The dust temperature is thus determined by the aforementioned heating and cooling mechanisms and it typically has values around 12K (Bergin and Tafalla, 2007).

1.2 Chemistry of CH_3OCHO

Methyl formate (CH_3OCHO), regarded by astronomers as a complex molecule, is an organic molecule comprised of eight atoms belonging to a group of chemical compounds known as esters of which it is the simplest example (Reutemann and Kieczka, 2000). Its discovery in the ISM dates back to 1975 (Brown et al., 1975), where the emission line corresponding to the transition $1_{0,1} - 1_{1,1}$ at a frequency of 1.61 GHz was observed in Sagittarius B2, a giant molecular cloud located around 120 parsecs from the center of the Milky Way galaxy. It is but one of several organic compounds containing the methyl group (-CH_3) such as methanol (CH_3OH), formic acid (CH_3COOH) and acetaldehyde (CH_3CHO) to have been detected in the ISM. Besides Sagittarius B2, methyl formate is found in hot interstellar cores, corinos, the galactic center cloud and has even been detected in the Large Magellanic Cloud (Sewiło et al., 2018). Hot cores denote regions hot (T> 100K) and dense ($n_H = 10^{6-8}cm^{-3}$) regions within molecular clouds where high-mass protostar formation is ongoing. Hot corinos, in contrast to hot cores, are regions associated with the formation of lower and solar-mass protostars (Ceccarelli, 2008). They are cooler (T≈ 100K), but have similar densities. Corinos are also called "chemical-rich protostellar envelopes" given that they contain many organic compounds including complex molecules and ices. In 2012 Bacmann et al., 2012, after using the IRAM 30m telescope, announced the discovery of methyl formate in the cold prestellar core L1689B. Fractional abundances with respect to molecular hydrogen are $10^{-9} - 10-8$ for hot cores and corinos and $10^{-11} - 10-10$ in dark clouds.

The formation of methyl formate is far more nuanced than that of NH and ND, and there is still much uncertainty surrounding it. It was initially thought that methyl formate is a first-generation species, meaning that it forms during the warm-up phase, which denotes the period in

time during which a cold (molecular) core transitions into a young stellar object (YSO) (Herbst and Van Dishoeck, 2009). During the cold core era, large molecules, most notably methanol and formaldehyde, may form on the surfaces of dust grainss. During the warm-up period, photodissociation of the aforementioned zeroth-generation molecules produces radicals such as CH_3O and HCO which are able form larger molecules, like methyl formate, through associative reactions on grain surfaces and in the gas phase (Garrod and Herbst, 2006). Further granular surface reactions are proposed in Garrod et al., 2008). The warm-up phase is succeeded by the hot core or corino phase, hence why methyl formate is abundant in these regions. However, the detectable presence of methyl formate in cold cores strictly implies the existence of more formation mechanisms. To explain the abundances, Vasyunin and Herbst, 2013 proposed the gas-phase reaction between the methyl (CH_3) and methoxy (CH_3O) radicals. Methyl formate is also deemed a "pre-biotic" molecule due to the fact that it's possible for it to be involved in reactions to form larger and more complex molecules, eventually leading to the formation of biomolecules which are preconditions for life to form (Faure et al., 2011).

1.3 Interstellar line spectra

Thus far, the detection of NH and ND has always followed through absorption spectroscopy. However, molecules, or interstellar clouds in general, can also be observed thanks to their emission spectra, as has been observed for methyl formate. For this to occur, however, the molecules, atoms or ions within a gas cloud must first enter excited states. This can happen either through radiative, or collisional excitation. Radiative excitation is the process by which a molecule, for instance, absorbs a photon, which increases its internal energy and thus it enters an excited state. In diffuse and non-shielded regions of the ISM, radiative excitation is by far the dominant process by which interstellar species are excited (Maciel, 2015). In dense and shielded regions, however, radiative excitation's prominence declines significantly and the contribution of collisional excitation becomes very significant, meaning that one has an interplay of radiative and collisional processes. Collisional excitation occurs when interstellar species collide inelastically with one another, meaning that some of the kinetic energy of the collision partners before the interaction is transformed into internal energy as a result of the collision. Typical collision partners in the ISM are hydrogen in all its stable forms, helium and electrons (Draine, 2011). For molecular clouds, the most prominent collision partner is, unsurprisingly, H_2. Collisions with molecular hydrogen induce NH, ND and methyl formate to enter higher rotational states, which will be dealt with in due time. De-excitation, translating to the emission of a photon, follows either by spontaneous emission or through the reverse process known as collisional de-excitation.

The observation of (sub)millimeter wavelength spectral lines, as is the case for NH, ND and methyl formate, are powerful tools to probe both the physical conditions and chemical processes that are ongoing in their respective astronomical sources, especially when local thermodynamic equilibrium is no longer a valid assumption (van der Tak et al., 2007). To properly understand the emergence of spectral lines through both radiative and collisional excitation, one requires

extensive calculations which take both collisional and radiative processes into account. However, especially on the collision side, the input data is fairly often missing or limited in terms of its coverage of energy states and temperature range. It wasn't until fairly recently that this was the case for NH, ND and methyl formate. Breakthroughs were made by Toboła et al., 2011 and Dumouchel et al., 2012, who computed the collisional cross sections of NH and ND, and Faure et al., 2014 who did the same for methyl formate. They were subsequently able to obtain the collision rate coefficients for collisions of the respective species with Helium. With the collision data available, investigating the spectral lines of these species is now possible with more precision than ever before.

1.4 Goals of this thesis

Gaining knowledge and understanding of interstellar NH, ND and CH_3OCHO with regards to radiative and collision processes is imperative. Observations and investigations of spectral lines of the aforementioned species, will lead to refinements of chemical models (Le Gal et al., 2014, Herbst and Van Dishoeck, 2009) that not only lead to the molecules' own formation, but also to the formation of other compounds. Inferring abundances from observations can be quite tricky, especially when assumptions regarding collisional processes have to be made.

This project aims at facilitating this process by enabling the inference of NH, ND and and CH_3OCHO column densities based on calculated spectral features that factor in the physical conditions of the medium which the molecules populate. To achieve this, the line strengths of the molecular emissions will be investigated as functions of column density, as well as the impact of ambient physical conditions have on that relation. The physical conditions in question are the kinetic temperature, the molecular hydrogen density and, in the case of dark clouds, the dust temperature. Furthermore, since learning from molecular spectra relies significantly on observation, the radiative transitions corresponding to the strongest lines will be selected and tested in terms of their detectability by modern instruments. Hence, constraints will be sought on the physical parameters and abundances that could lead to the detection of the emission or absorption spectra of NH, ND and CH_3OCHO.

The differences in terms of molecular emissions between NH and ND will be looked at as well. There is still much uncertainty surrounding both the ND/NH and NH/N abundance fractions. The aim is thus to provide the means to improve these estimates.

The following section is intended as means of familiarization with the theoretical aspects of collisional excitation and radiative processes, both of which are key in the emergence of molecular emissions and absorptions if a radiation field is present. Most equations and content, unless stated otherwise, were taken from van der Tak et al., 2007. Subsequently, in the context of rotational spectroscopy, the molecules themselves will be considered at in more detail, namely their geometry and their rotational levels.

2 Formalism

2.1 Collisional excitation

As alluded to earlier (1.3), collisional excitation is the process by which interstellar atoms, ions and molecules enter excited energy states after colliding inelastically with one another, implying that some of the kinetic energy before the collision is transformed into internal energy. The reverse process is known as collisional de-excitation, meaning that species in excited states collide and gain kinetic energy while transitioning down to a lower energy state. De-excitation can also occur spontaneously due to the fact that its more energetically efficient for any species to find itself in a lower state. As stated, in molecular clouds molecules collide with H_2, the most abundant constituent of such regions, and the collisions induce molecules to become collisionally excited. The rate at which collisions occur between upper levels u and lower levels l is given by:

$$C_{ul} = n_{col}\gamma_{ul} \tag{1}$$

Where, n_{col} (cm^{-3}) denotes the number density of the collision partner and γ_{ul} (cm^3/s) represents the downward collision rate coefficients, meaning it deals collisionally induced de-excitation as the transitions is from an upper level to a lower one ($u \rightarrow l$). The upward collision rate coefficient, γ_{lu}, is related to its downward counterpart through statistical equilibrium:

$$\gamma_{lu} = \gamma_{lu}\frac{g_u}{g_l}e^{-h\nu/k_B T_{kin}} \tag{2}$$

Here, g_i refers to the statistical weight of the levels, h is Planck's constant, ν corresponds to the frequency of a photon that is emitted in a downward transition with the energy of that photon being $E = h\nu$, k_B is Boltzmann's constant and T_{kin} is the kinetic temperature of the gas. The collision rate coefficients themselves are the velocity-integrated collision cross section σ with the downward rate given by:

$$\gamma_{ul} = \left(\frac{8k_B T_{kin}}{\pi\mu}\right)^{-1/2}\left(\frac{1}{k_B T_{kin}}\right)^2 \int \sigma E e^{-E/k_B T_{kin}}\, dE \tag{3}$$

Here, μ represents the reduced mass of the collision system. The key quantities and dependencies for the rate coefficients are the kinetic temperature and of course the collision cross section, which itself is a function of the collision energy E, i.e. kinetic energy , with $E = \mu v^2/2$ and v being the velocity. Effectively, the collisional cross section is the quantity denoting the probability of a collision occurring. As stated previously (1.3), the collision cross section for the interstellar species NH, ND and methyl formate weren't known until fairly recently, and determining the aforementioned quantity is quite a challenge. It requires the modeling of a potential energy surface (PES) (Roueff and Lique, 2013) which can be obtained using *ab initio* quantum mechanical methods. The PES can subsequently be used as the potential function in the Schrödinger equa-

tion to derive the cross sections and rate coefficients correspondingly based on a time-independent quantum formalism, called "close-coupling" (CC), where the various rotational wave functions are solutions of coupled second order differential equations. It isn't unusual for the computation of collision rate coefficients to be done with Helium as a collision partner, as the cross section for that collision is far easier to compute given that the PES for Helium is less complex than that of H_2. Therefore, obtaining accurate coefficients for systems with H_2 as the collision partner is quite difficult and requires complicated and extensive calculations. To get an estimate for the rate coefficients for a system where He is substituted by H_2, one may scale the rates according to the equation below (Schoeier et al., 2005).

$$\gamma_{X-H_2} = \gamma_{X-He}\sqrt{\frac{\mu_{X-He}}{\mu_{X-H_2}}} \tag{4}$$

X refers to the molecular species for which the rate coefficients have been computed and μ designates the reduced mass of the respective collision system. Scaling the coefficients in this manner is an approximation and that the scaled coefficients aren't guaranteed to be accurate (van der Tak et al., 2020). Collision with He don't necessarily translate to a system were He is substituted with H_2.

In collisionally excited regions of the ISM, the molecules of a certain species may occupy many different energy levels. The number density ratio between a population in an upper levels u and a lower level l is given by the Boltzmann equation, much like the rate coefficients:

$$\frac{n_u}{n_l} = \frac{g_u}{g_l} e^{-(E_u - E_l)/k_B T_{ex}} \tag{5}$$

It is important to note that the kinetic temperature is replaced here by a quantity known as the excitation temperature T_{ex}. This is due to the fact that local thermodynamic equilibrium isn't achieved in most regions of the ISM, especially diffuse ones. The excitation temperature is thus defined as the temperature of the Boltzmann factor responsible for a certain abundance ratio. Generally speaking, the excitation temperature differs between lines of the same molecule. If LTE is achieved, then the excitation temperature is equal to the kinetic temperature, otherwise, it is smaller. This can be deduced from how they are related (Roueff and Lique, 2013):

$$T_{ex} = T_{kin} \cdot \left(1 + \frac{k_B T}{E_u - E_l} \cdot \frac{A_{ul}}{n k_{ul}}\right)^{-1} \tag{6}$$

The number densities in equation 5 may also be replaced by a very important quantity known as column density N (cm^{-2}). The column density is the number density of any interstellar species integrated along the line of sight of a medium ($N = \int n\, ds$). The derivation of a species' column density is crucial if one wants to determine its abundance. This can be done by analyzing the emission spectra, which is directly linked to the population of the upper level.

2.2 Radiative Transfer

To describe the transfer of radiation, one requires a quantity that remains constant, unless absorption or emission processes occur along the travelled direction. The quantity known as specific intensity I_ν satisfies these conditions. It has units (erg $s^{-1}cm^{-2}Hz^{-1}sr^{-1}$), meaning it encapsulates the amount of energy passing through a surface normal to the path of travel per unit time, area, bandwith and solid angle. The radiative transfer equation is given below.

$$\frac{dI_\nu}{ds} = j_\nu - \alpha_\nu I_\nu \tag{7}$$

What equation (7) represents is the change in specific intensity I_ν that radiation undergoes after traversing some sort of medium. The change in specific intensity, as stated, can result from emission and absorption occurring within that medium with the former's coefficient given by j_ν and the latter's by α_ν.

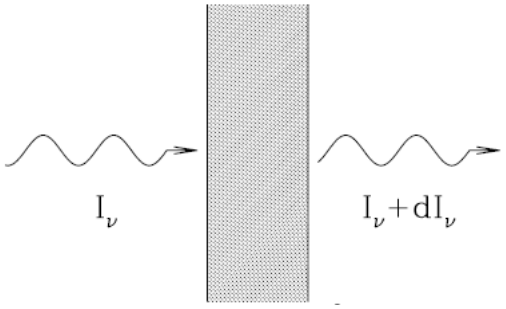

Figure 2: Radiative transfer geometry. A beam of specific intensity I_ν traverses a medium (gray-dotted region) resulting in a change of the beam's intensity dI_ν after the medium has been traversed. The image was taken from Maciel, 2015.

The radiative transfer equation, in the context of the ISM, is ordinarily used to describe the absorption and attenuation of stellar radiation as it passes through interstellar clouds. The clouds themselves, of course, may also produce their own emissions if radiative and/or collisional excitation occur within them. In the absence of a strong radiation field, meaning that $I_\nu \approx 0$, only the emission coefficient j_ν of radiative transitions happening in the cloud is of note and it is defined as:

$$j_\nu = \frac{h\nu_{ul}}{4\pi} n_u A_{ul} \phi_\nu \tag{8}$$

A_{ul} is the Einstein coefficient responsible for spontaneous emission, meaning that it expresses the probability of the transition occurring within a certain time interval. The number density of molecules in the upper level is given by n_ν. ϕ_ν represents the emission line profile, which is most commonly a Doppler profile, meaning that it arises due to the relative motion of the molecules themselves. In cold and dark cloud cores, however, the profile is that of a Gaussian given that the broadening is ascribed to turbulence occurring in those regions.

What equation (7) and figure (2) also imply is that photons, which may originate from stars or produced via de-excitation of interstellar species, that traverse interstellar clouds aren't guaranteed to make it out of the cloud. It is therefore conventional to quantify an escape probability for a photon passing through an interstellar cloud. If the medium is assumed to be a uniform sphere, the escape probability β is given by (Osterbrock and Ferland, 2006):

$$\beta_{sphere} = \frac{1.5}{\tau}\left[1 - \frac{2}{\tau^2} + \left(\frac{2}{\tau} + \frac{2}{\tau^2}\right)e^{-\tau}\right] \tag{9}$$

The dimensionless quantity τ is a geometric means of quantifying the optical opaqueness of a medium. For τ
$ll1$, the medium is optically thin, meaning than the majority of the radiation passing through the medium is transmitted. In other words, the escape probability will essentially be equal to one, meaning that photons will barely interact with the medium. Conversely, if τ
$gg1$, the medium is said to be optically thick and a photon stands very little chance of escaping.

The flux F_ν (ergcm^{-2}s^{-1})of that emission line is then the velocity-integrated intensity. The flux can also be computed from the formula below :

$$F_\nu = \frac{\sqrt{\pi}}{2\sqrt{\ln 2}} T_R \Delta V \tag{10}$$

T_R refers to the radiation temperature and ΔV to the full width at half maximum (FWHM) of the Gaussian line profile. The radiation temperature is defined as the temperature such that a blackbody at that temperature would have the same specific intensity $B_\nu(T_R) = I_\nu$ as the emission line within the Rayleigh-Jeans limit which corresponds to a lower range of frequencies. The magnitude of T_R is also dependent on the intensity of the background radiation in the sense that for the same specific intensity of an emission line, a higher background radiation corresponds to a lower radiation temperature, as can be inferred from the following equation.

$$T_R = \frac{c^2}{2k_B\nu^2}(I_\nu^{em} - I_\nu^{bg}) \tag{11}$$

If the intensity of the background radiation exceeds that of the spectral line, the radiation T_R will be negative and so will the flux of the line. This means that the line is no longer resultant from emission, but rather a case of absorption, meaning that the spectral line is characterized by a dip in the continuum radiation spectrum instead of a spike.

2.3 Rotational Spectroscopy

Molecular radiative transitions are more complex than those of single atoms or ions, where the transition of electrons from higher energy to lower energy orbitals are the dominant source behind emission spectra. Molecules, on the other hand, can vibrate, rotate or even do both simultaneously. Rotational spectroscopy concerns itself with measuring both the energies and transitions

between quantized rotational states of molecules. Radiation resulting from such transitions ordinarily fall into the (sub)millimeter and infrared range of the electromagnetic spectrum. The rotational states of a molecule can be derived by solving the Schrödinger equation.

2.3.1 NH, ND

NH and ND are both linear diatomic molecules with masses of 15 and 16 amu [1], respectively. Both have permanent dipole moments due to the nitrogen atom's electron cloud, with $\mu_{NH} = \mu_{ND} = 1.300D$[2]. The molecules each present two unpaired electrons of spin 1/2, meaning that the total spin angular momenta can take values of $S = 0, 1$ and that spin-spin interaction must be accounted for, in addition to the standard coupling between spin angular momentum S and nuclear angular momentum N. This implies that the rotational levels of the isotopologues are split into spin-triplets states $^3\Sigma$ above the ground state, where $N = 0$. The triplet states are characterized by the quantum number J, the total angular momentum with $\mathbf{J} = \mathbf{N} + \mathbf{S}$ which reduces to $J = N,\ N \pm 1$ in this instance (Gordy and Cook, 1984). The energies of the rotational states are given by the equations below.

$$\frac{E_{J=N+1}}{h} = B_\nu N(N+1) + \gamma(N+1) - \frac{2\lambda(N+1)}{2N+3} \tag{12}$$

$$\frac{E_{J=N}}{h} = B_\nu N(N+1) \tag{13}$$

$$\frac{E_{J=N-1}}{h} = B_\nu N(N+1) - \gamma N - \frac{2\lambda N}{2N-1} \tag{14}$$

B_ν, γ and λ represent the rotational constant, the spin-rotation constant and the spin-spin interaction constant, respectively. The values used by Toboła et al., 2011 and Dumouchel et al., 2012 can be found in these respective resources (Takano et al., 1998 and [3]). The selection rules for the radiative transition between rotational levels are as follows.

$$\Delta N = \pm 1 \qquad\qquad \Delta J = 0, \pm 1 \tag{15}$$

[1] http://udfa.ajmarkwick.net/index.php?species=23
[2] https://webbook.nist.gov/cgi/cbook.cgi?Source=1965IRW%2FDAL1766&Mask=1000
[3] https://physics.nist.gov/PhysRefData/MolSpec/Diatomic/Html/Tables/NH.html

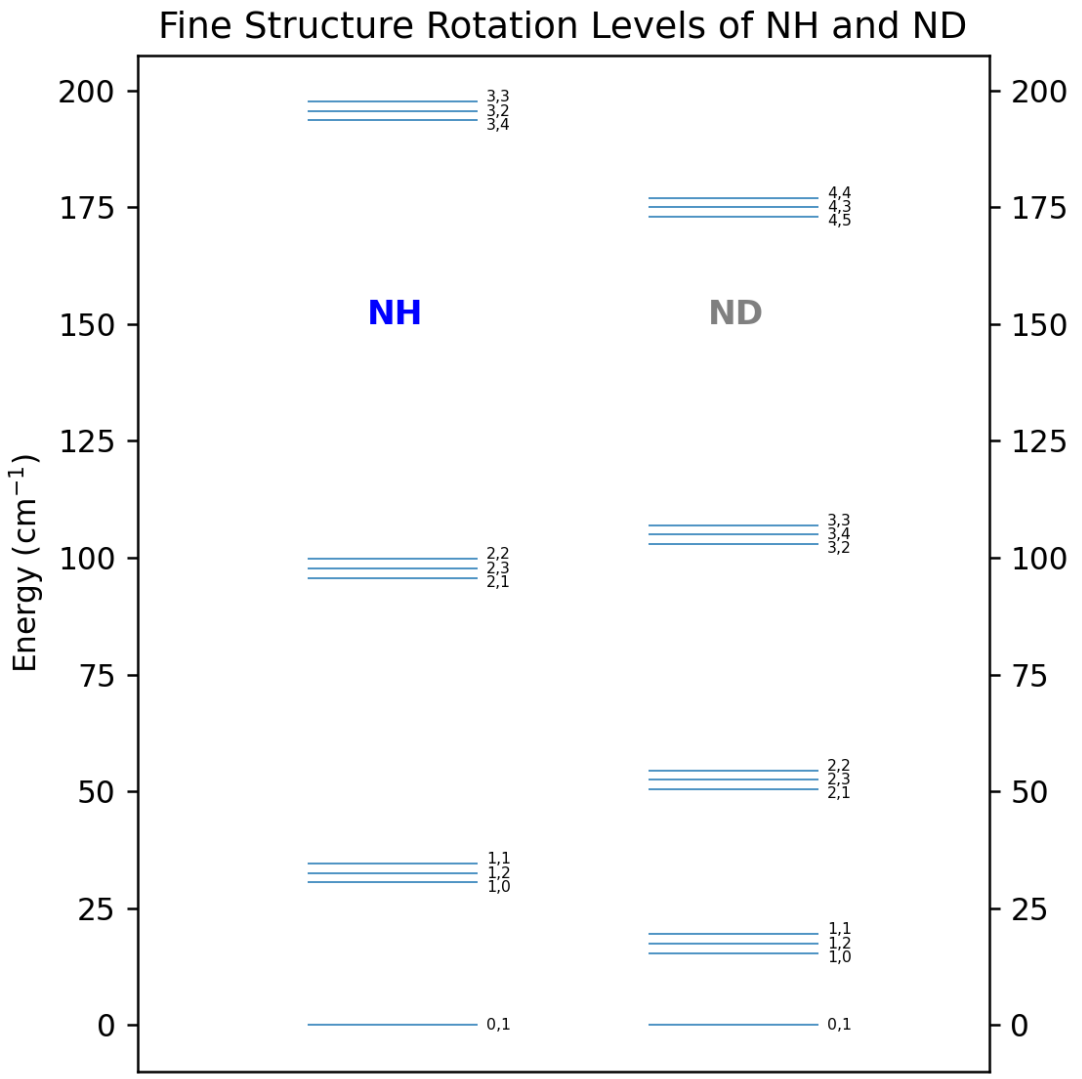

Figure 3: Energy diagram of the first 10 levels of NH on the left and the first 13 levels of ND on the right. The spacing between the individual triplets is not to scale here and was enlarged for this diagram. The narrower spacing between the ND levels is due to the fact that the rotational constants for ND are smaller than their NH counterparts. The levels are labeled according to the quantum numbers N, J. One may also realize that for $N = 4$, the $J = N + 1$ level is lower in energy than the $J = N - 1$ level for ND whereas otherwise, the $J = N + 1$ level for each N is higher in energy. This also applies to NH, though the $N = 4$ levels aren't shown here.

2.3.2 Methyl Formate

CH_3OCHO is a prolate asymmetric top molecule (Faure et al., 2011) with a mass of 60 amu. The asymmetry derives from the fact that none of the molecule's principal moments of inertia are equal to each other and due to there being no axis of symmetry within the molecule itself. The structural isomers of methyl formate are glycolaldehydea and acetic acid (Faure et al., 2011),

both of which have been detected in the ISM, with the former and latter being one and two orders of magnitude less abundant than than their isomeric ester in hot cores and corinos (Hollis et al., 2000). The molecule also displays two conformers, namely *cis*- and *trans*-methyl formate (see below) with the former being more stable and consequentially more abundant, although *trans*-methyl formate has also been detected in interstellar clouds (Neill et al., 2012).

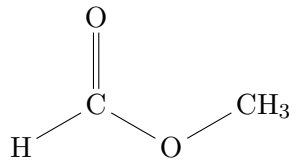

cis-methyl formate

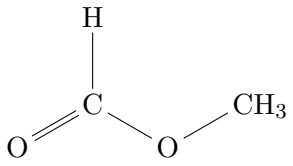

trans-methyl formate

For asymmetrical molecules, it is conventional to define a reference geometry as this greatly facilitates calculations involving angular momentum because it establishes the directional moments of inertia. Faure et al., 2011 defined the following reference position for methyl formate to obtain the PES which is a key component in finding the collisional cross section.

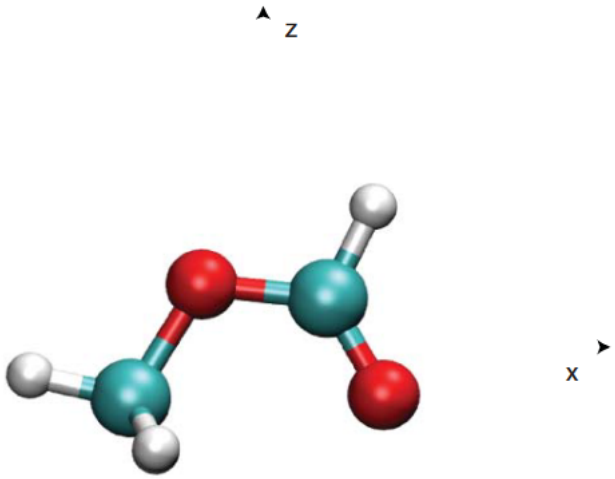

Figure 4: Reference position of methyl formate as defined by Faure et al., 2011.

Methyl formate is classified as a flexible molecule Kroto, 1992. This means that besides the standard complete rotation of the molecule in the context of rotational spectroscopy, one must also account for another type of motion, namely internal rotation. The prime internal rotor is ordinarily the methyl group, though it has to be noted that its rotation is very often restricted in some way, as is the case for methyl formate. With the necessary boundary conditions in place, one may solve the torsional Hamiltonian, which deals with the twisting of the molecule, to

obtain the torsional wavefunctions. The resulting functions are characterized by an index σ which determines the symmetry of these functions. If $\sigma = 0$, the functions are non-degenerate, but if $\sigma = \pm 1$, the functions are degenerate. Hence, one may distinguish between A (non-degenerate) or E (degenerate) species. In the case of methyl formate, each rotational level is subsequently divided into a non-degenerate A-level and a degenerate E-level. The margins between A and E-type methyl formate, however, are extremely small, with A-type and E-type radiative transitions differing by less than 0.1 cm^{-1} (Faure et al., 2014). With the collisional cross sections of the two symmetries being also nearly identical, they can be considered analogous systems, an thus A-type methyl formate will be at the forefront of any calculation.
The rotational levels of methyl formate are characterized by three numbers, namely the quantum number J, which denotes the total angular momentum, and the pseudo-quantum numbers K_a and K_c. The two latter are nothing other than the projections of J along the x-axis and y-axis. The standard selection rules for the radiative transitions are (Faure et al., 2014):

$$\text{a-type:} \qquad \Delta J = 0, \pm 1 \qquad \Delta K_a = 0 \qquad \Delta K_c = \pm 1 \tag{16}$$

$$\text{b-type:} \qquad \Delta J = 0, \pm 1 \qquad \Delta K_a = \pm 1 \qquad \Delta K_c = \pm 1, \pm 3 \tag{17}$$

The letters a and b are in reference to two distinct inertia axis corresponding to the x and z axis in the context of the molecular plane shown in figure (4).

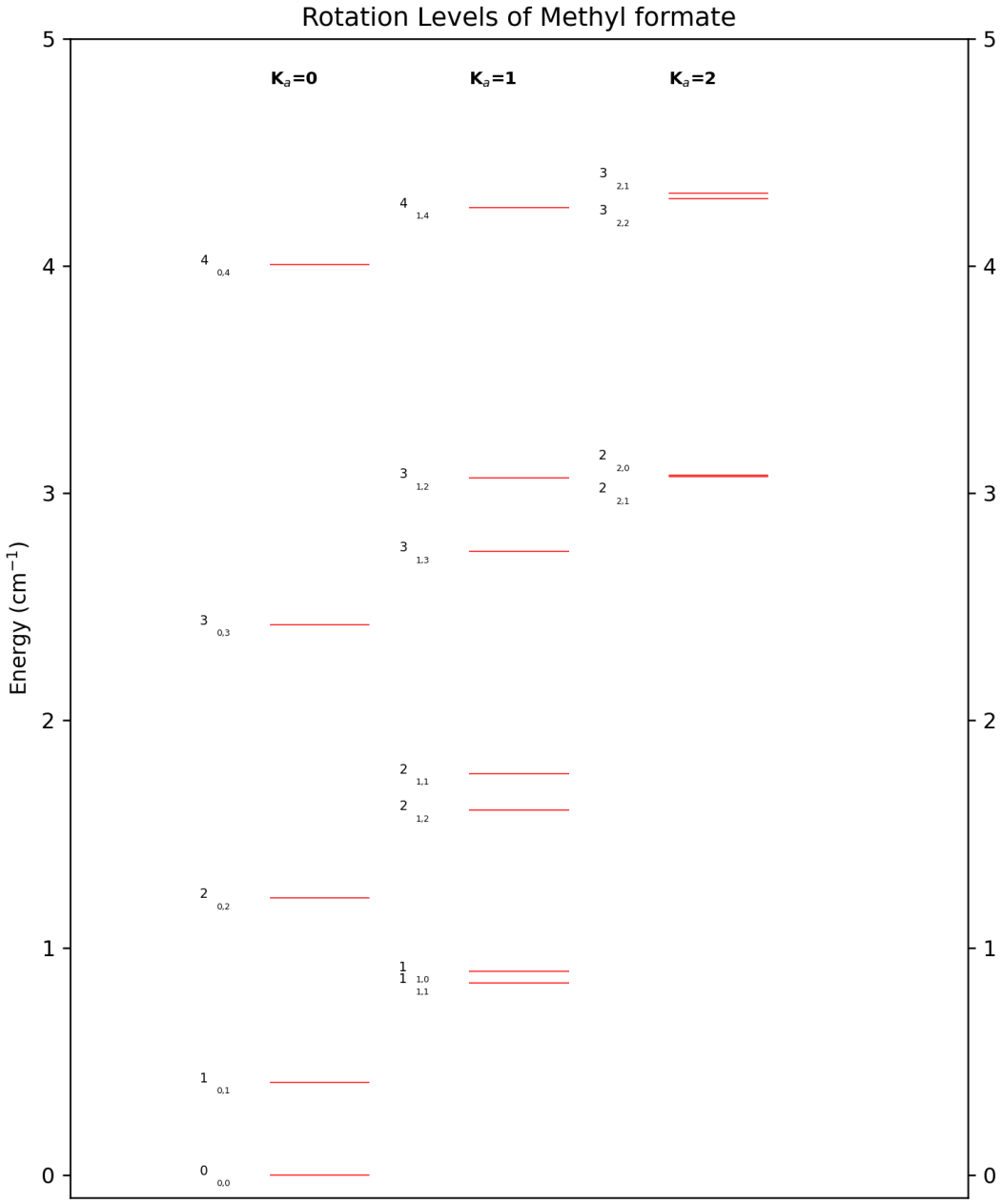

Figure 5: The figure above shows the first 16 rotation levels of methyl formate. The numbers next to the line levels follow the notation:J_{K_a,K_c}

3 Methods

3.1 Construction of Molecular Data Files

The initial phase of the project consisted of unifying the spectroscopic and collisional data of the molecules within designated data files in LAMDA format. LAMDA [4] (van der Tak et al., 2020), the Leiden Atomic and Molecular Database, is a database that aims to provide basic atomic and molecular data required to perform excitation calculations in radiative transfer codes such as Radex [5]. The files contain information about the energies of the rotational levels in units of cm^{-1} and their statistical weights, the possible radiative transitions between the rotational levels along with their Einstein A-coefficients which encapsulate the probability of spontaneous downward transitions, and of course the collisional de-excitation rate coefficients as well as their respective temperatures.

For NH, the fine structure rotational levels and the collisional de-excitation rate coefficients with Helium, computed by Toboła et al., 2011 for a temperature range spanning $5K - 350K$, were readily available on the BASECOL database [6]. The rotational levels and the ND-He rate coefficients for temperatures $5K - 150K$ were taken from Dumouchel et al., 2012. Given that NH and ND are found in molecular clouds within the ISM, the rate coefficients had to be adjusted to account for collisions with H_2 instead of He. This was done by scaling the coefficients with the square root of the ratio between the reduced masses of the NX-He and NX-H_2 systems, as detailed in equation (4). As touched upon previously (4), the scaled coefficients are simply approximations and accuracy isn't necessarily guaranteed. The Einstein coefficients for the transitions of NH and ND were obtained from the CDMS database [7]. The spectroscopic data from the CDMS database factored in the hyperfine structure of the isotopologues. The collision data, however, only considered the fine structure of the molecules. Since the hyperfine splitting is around a factor of 1000 smaller than the fine structure counterpart (Dumouchel et al., 2012), they could be considered degenerate with respect to the fine structure scale and subsequently, the Einstein coefficients of the hyperfine transitions were added together to approximate the corresponding fine structure transition.

For A-type methyl formate, a data file compiled by Faure et al., 2014 was readily available.

[4] https://home.strw.leidenuniv.nl/~moldata/
[5] https://home.strw.leidenuniv.nl/~moldata/radex.html
[6] https://basecol.vamdc.eu/index.html
[7] https://cdms.astro.uni-koeln.de/classic/entries/

```
!MOLECULE (Fine rotational levels of NH (as used in Tobola et al (2011) from
    BASECOL)
NH
!MOLECULAR WEIGHT
15
!NUMBER OF ENERGY LEVELS
25
! Level  +  Energy(cm-1) +  Weight + QNUM. (N J) +  SpinComponentLabel
       1       0.000000        3.0      0.0  1.0              1
       2      31.570602        1.0      1.0  0.0              3
      (etc)
      25    1168.502044       17.0      8.0  8.0              2
!NUMBER OF RADIATIVE TRANSITIONS
45
!TRANS +   U +   L + A(s^-1) +       FREQ(GHz) +     E_up(K)
     1     2     1  0.01301294       946.4611887    45.4238
     2     3     1  0.04166734       974.4727948    46.7676
    (etc)
    45    25    20  0.46403554       7774.4701669   1681.24
!NUMBER OF COLL PARTNERS
1
!COLLISIONS BETWEEN
1  NH - H2 (scaled from NH - He coefficients from Tobola et al (2011))
!Number of collision transitions:
300
!Number of collision temperatures:
23
!COLL TEMPS:
5.0 10.0 20.0 30.0 40.0 50.0 60.0 70.0 80.0 90.0 100.0 120.0 140.0 160.0 180.0
    200.0 220.0 240.0 260.0 280.0 300.0 320.0 350.0
!Trans + Upper + Lower + COLLRATES(CM^3S^-1)
1  2  1  1.5135e-12 1.1392e-12 1.0718e-12 1.2183e-12 1.4272e-12 1.6739e-12
    1.9556e-12 2.2715e-12 2.6197e-12 2.9978e-12 3.4029e-12 4.2806e-12 5.2281e-12
     6.2235e-12 7.2490e-12 8.2907e-12 9.3373e-12 1.0381e-11 1.1414e-11 1.2434e
    -11 1.3436e-11 1.4417e-11 1.5847e-11
2  3  1  2.4519e-12 2.0825e-12 1.9390e-12 1.9837e-12 2.0707e-12 2.1753e-12
    2.2940e-12 2.4261e-12 2.5710e-12 2.7286e-12 2.8979e-12 3.2675e-12 3.6717e-12
     4.1023e-12 4.5522e-12 5.0154e-12 5.4869e-12 5.9628e-12 6.4396e-12 6.9151e
    -12 7.3871e-12 7.8539e-12 8.5421e-12
(etc)
300  25  24  3.9033e-13 4.6615e-13 6.8249e-13 9.3617e-13 1.2125e-12 1.5054e-12
    1.8112e-12 2.1268e-12 2.4500e-12 2.7789e-12 3.1119e-12 3.7849e-12 4.4611e-12
     5.1349e-12 5.8025e-12 6.4614e-12 7.1098e-12 7.7466e-12 8.3708e-12 8.9819e
    -12 9.5795e-12 1.0163e-11 1.1011e-11
```

Table 1: Snippet of the data file for NH in LAMDA format. As a matter of convenience, the majority of the rotational levels, radiative transitions and collision rate coefficients were removed.

3.2 Computation of Spectral Features in Interstellar Clouds

The subsequent phase of the project consisted of running the files through RADEX, a computer program for fast non-LTE analysis of interstellar line spectra (van der Tak et al., 2007). Used as part of the LAMDA database, it calculates the strengths of calculate the strengths of atomic and molecular lines from interstellar clouds which are assumed to be homogeneous. It utilizes the escape probability formulation to consider the global properties of interstellar clouds and how likely it is for a photon to escape the cloud. The code contains three escape probability methods that differ in their geometric assumptions. For this project, a static, homogeneous and spherically symmetric medium was assumed, which falls under the method denoted as *uniform sphere*. More on the other available methods can be found in van der Tak et al., 2007, and for the uniform sphere method in Osterbrock and Ferland, 2006.

For NH and ND, conditions in diffuse molecular and cold dark clouds were simulated. For methyl formate, on the other hand, the same was done but solely with conditions prevailing cold dark clouds given that the collision rate coefficients were only available for temperatures for $5\text{K} - 30\text{K}$. The table below shows a summary of most the parameters that were fed into RADEX with the help of a python script. The parameters not included were the line width, which was assumed to be $\Delta v = 0.6$ kms^{-1} for all calculations and species, and the background temperature. Values for the latter took the form of the CMB temperature (2.73 K) for all conditions, but also assumed values of 8 K and 12 K to simulate dust temperatures in dark clouds.

Table 2: RADEX Input Parameters

Medium	T_{kin} (K)	$n(H_2)$ (cm^{-3})	ν (GHz)	N_{mol} (cm^{-2})	Species
Diffuse Molecular Clouds	$30 - 100$	$100 - 500$	$480 - 2000$	$1 \cdot 10^{12} - 7 \cdot 10^{14}$	NH & ND
Cold Dark Clouds	$10 - 20$	$10^3 - 10^5$	$480 - 2000$	$1 \cdot 10^{12} - 7 \cdot 10^{14}$	NH & ND
			$84 - 116$	$1 \cdot 10^{11} - 7 \cdot 10^{13}$	Methyl Formate

For each set of input parameters, RADEX compiled a file containing the computed results for each spectral line in the given range of frequencies. The range of frequencies was selected based on the bands of the Herschel HIFI instrument [8] for NH and ND, and the ALMA (Atacama Large Millimetre/Submillimetre Array) telescope [9] for methyl formate, respectively. The HIFI instrument has already been used to detect NH and ND in the interstellar medium. It completely covers the frequency ranges 480-1250 GHz and 1410-1910 GHz. The first range is split into five bands and the second into two bands. Moreover, each band is split into "a" and "b" components. One may note that the frequency range for NH and ND indicated in the table 2 goes beyond that of the HIFI instrument. This was done in order to include the radiative transitions of NH

[8] http://herschel.esac.esa.int/Docs/HIFI/html/hifi.html
[9] https://almascience.eso.org/documents-and-tools/cycle10/alma-technical-handbook

between the N= 2 and N= 1 triplets, which have frequencies between 1920 GHz and 1990 GHz. The frequency range selected for methyl formate corresponds to the range of band 3 of the ALMA telescope.

The column densities for NH and ND were selected according to the range of abundances that were detected or calculated, and presented in various papers. The largest NH column density to have been detected was reported by Hily-Blant et al., 2010 figured at $(2.20 \pm 0.80) \cdot 10^{14}$ cm^{-2} and the lowest by Meyer and Roth, 1991 coming in at $9.0 \cdot 10^{11}$. The calculations went beyond the maximum value in order to account for abundances that may exceed the present limit. Given that Bacmann et al., 2010 estimated the ND/NH fraction to be up to 100%, the same column densities were selected for NH and ND. In dark clouds, methyl formate is estimated to have a fractional abundance of $10^{-11} - 10^{-10}$ with respect to molecular hydrogen. H_2 has column densities of approximately 10^{23} cm^{-2}, not excluding one order of magnitude above or below.

The analysis of the outputs from RADEX continued in several phases. First, the two hydrides were considered. Both the influence of temperature and molecular hydrogen density were investigated. After that, the radiative transitions producing the highest line strengths and fluxes were inferred. Subsequently, the difference in excitation between the isotopologues was looked at. Then, observational constraints were determined for NH and ND in diffuse molecular clouds. This consisted of finding the minimum required column density for a given set of physical parameters at which the line strength of a radiative transition surpassed 1 mK. The HIFI instrument has detected emission lines down to that order of magnitude (Weiß et al., 2010), though this was for an intergalactic study. 1 mK is admittedly a very optimistic lower limit for detections with modern instruments. Detecting radiation temperatures that faint within the Milky Way is at present highly improbable and is reserved for future telescopes which will undoubtedly be much more powerful and sensitive.

Once that was completed, the radiative transitions of NH and ND in dark cloud conditions were considered and the effect the dust temperature has on such a system. Next, observational constraints with dark cloud conditions in place were determined following the same strategy as was done for diffuse clouds.

Finally, an estimate of the NH/N fraction was made based on the findings.

For methyl formate, as stated, only dark cloud conditions were implemented due to the fact that firstly, it hasn't been found in diffuse clouds and secondly, the rate coefficients computed by Faure et al., 2014 only go up to 30 K. Since methyl formate presents a large amount of radiative transitions within the range of frequencies of ALMA,s band 3, six lines were selected to be at the forefront of focus. The lines were chosen based on their radiation temperatures that were found after several iterations of running the methyl formate data file through RADEX, with higher magnitudes favoured, and their frequency, such that lines spanning the entire ALMA band could be sampled. Of the six selected lines, two were the same as the ones as detected in Bacmann

et al., 2012, namely the 100.49 GHz and 100.68 GHz. The frequencies of the selected lines as well as the quantum numbers corresponding to the transitions are shown in the table below.

Table 3: Chosen methyl formate lines

Frequency (GHz)	88.85	90.16	90.23	100.49	100.68	111.68
$J_{K_a,K_c} \rightarrow J'_{K'_a,K'_c}$	$7_{1,6} \rightarrow 6_{1,5}$	$7_{2,5} \rightarrow 6_{2,4}$	$7_{0,8} \rightarrow 6_{0,7}$	$8_{1,7} \rightarrow 7_{1,6}$	$9_{0,9} \rightarrow 8_{0,8}$	$9_{1,8} \rightarrow 8_{1,7}$

The effects of dust temperature, once at 8 K and once at 12 K, were then investigated. After that, observational constraints for dark cloud conditions were derived, analogously as was done for NH and ND. The minimum line strength for methyl formate transitions to be detectable was taken to be 10 mK. Detecting signals that faint is possible with ALMA, given the appropriate resolution and integration time. For reference, a link to ALMA's sensitivity calculator is given here [10]. The minimally required column densities weren't derived for every individual line, instead, given that the excitation of the selected radiative transitions was very similar in general, they were grouped in the accordingly, 88.85-100.49 GHz and 100.68-11.68 GHz. Thus, it was for the groups of lines that the critical column densities were determined.

[10] https://almascience.nrao.edu/proposing/sensitivity-calculator

4 Results

4.1 Radiation Temperature and Flux as functions of Column Density

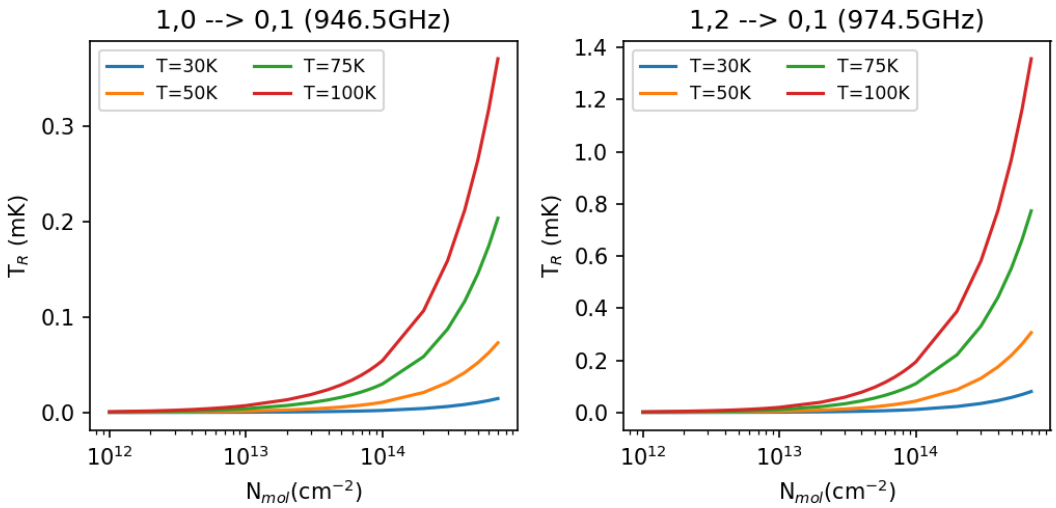

Figure 6: Radiation temperature T_R as a function of column density N (in logarithmic scale) at a molecular hydrogen density of $n(H_2) = 200$ cm^{-3} and a variety of temperatures, as indicated by the different colours for the first two radiative transitions of NH. All curves demonstrate that the radiation temperature increases with column density. Additionally, the radiation temperature also increases with the kinetic temperature of the gas, with a column density of 10^{13} cm^{-2} serving as the point at which the influence of kinetic temperature becomes significant.

.

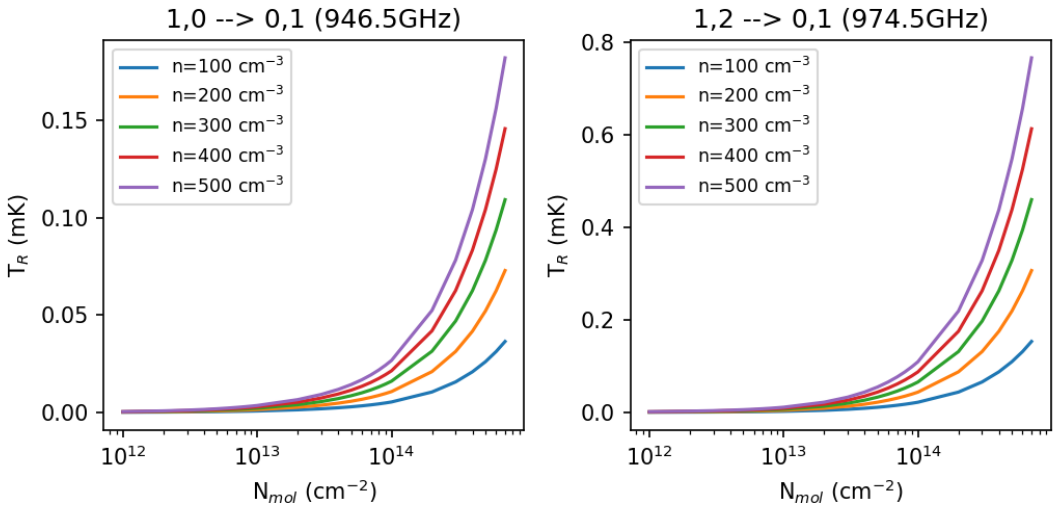

Figure 7: Radiation temperature T_R as a function of column density N (in logarithmic scale) at a kinetic temperature of $T = 200$K and a variety of hydrogen densities, as indicated by the different colours for the first two radiative transitions of NH. The same relation is observed as in figure (6). Additionally, the increase in number density has the same effect as increasing the kinetic temperature.

The flux of the emission lines as a function of column density follows the same relation as the radiation temperature. This can be derived from equation (10), where the dependence between the two quantities is linear. The lines for ND also display the same trend.

4.2 Strongest NH and ND Spectral Lines

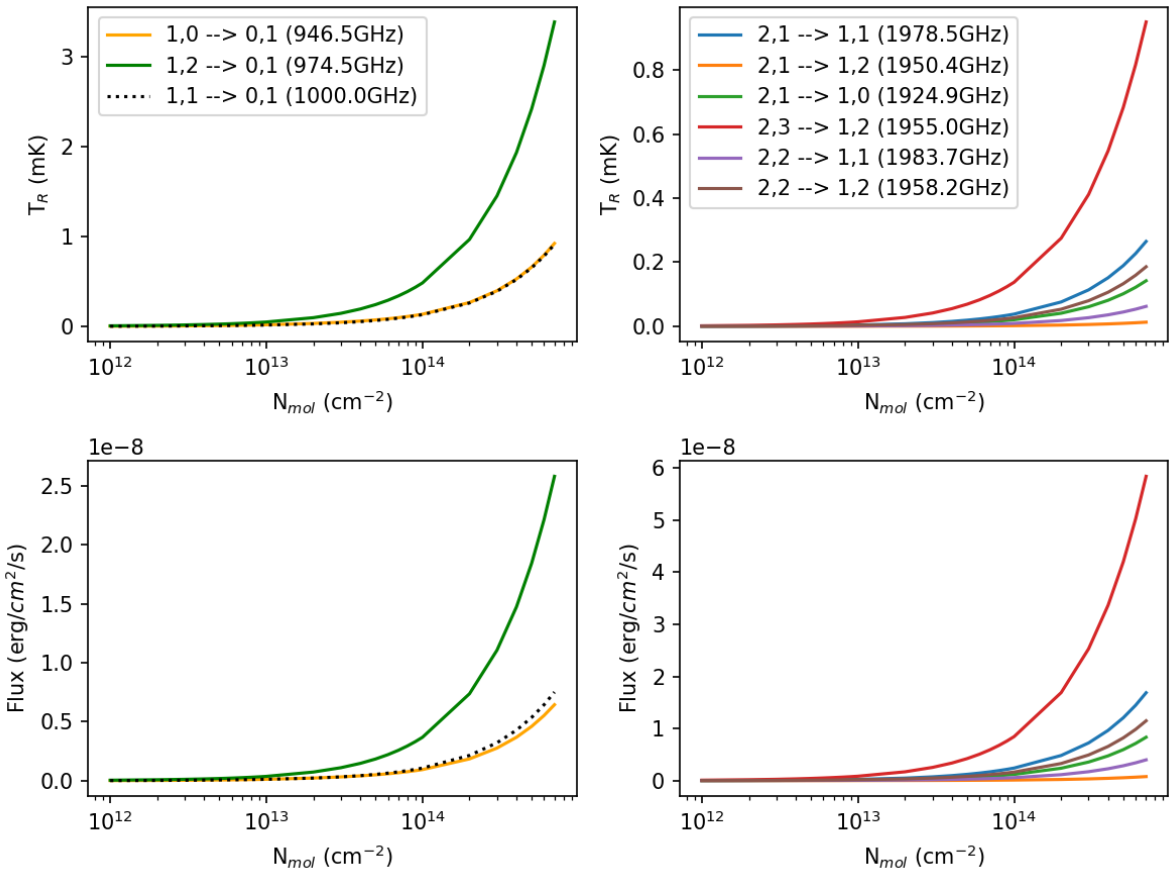

Figure 8: Radiation temperatures and fluxes as functions of column density of all radiative transitions of NH within the frequency interval specified in Table(2) at a $T_{kin} = 50$K and $n(\mathrm{H_2}) = 200$ cm^{-3}, which are conditions of diffuse molecular clouds.

It is clearly visible from figure (8) that the transitions to the ground state ($N = 1 \rightarrow 0$) produce the greatest line strengths. The 1955 GHz line yields the highest flux. This suggests that transitions from $N = 2 \rightarrow 1$ produce lines that are wider than their $N = 1 \rightarrow 0$ counterparts. Recalling from (10), the flux is defined as the velocity-integrated intensity. To produce radiative transitions between the first two excited states resulting from collisional excitation requires the collision partners to have more kinetic energy, which widens the line due to the effect of Doppler broadening. Also of note is the fact that the transitions following the pattern $\Delta N = -1$, $\Delta J = -1$ with $J = N + 1$ are the strongest for both transitions to the ground state and transitions to the first excited state. The underlying reason for this is that the Einstein A coefficients are larger for these types of transitions, meaning that the probability of spontaneous de-excitation is elevated compared to other downward transitions. Bearing all of this in mind, this makes transitions to the ground state as well as the 1955 GHz line of NH the best candidates for detection.

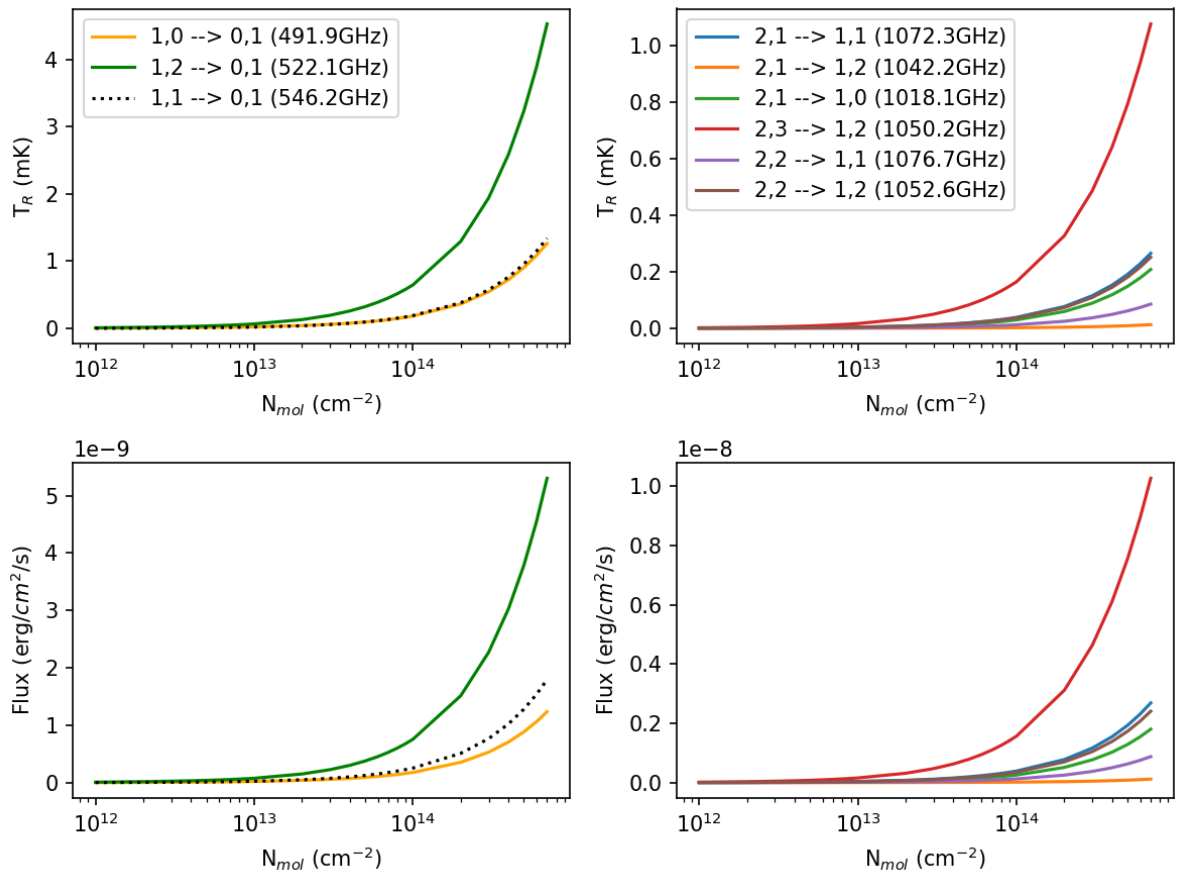

Figure 9: Radiation temperatures and fluxes as functions of column density of the first 9 transitions of ND within the frequency interval specified in Table (2) at a $T_{kin} = 50$K and $n(\mathrm{H_2}) = 200$ cm^{-3}, which are conditions found within diffuse molecular clouds

As is the case for NH, the transitions to the ground state produce the highest radiation temperatures. For the physical parameters in place, the 1050 GHz yields the highest flux out of all the lines. This isn't always the case, however. For lower kinetic temperatures and densities, it becomes more difficult for the molecule to access excited states beyond the first level. Moreover, much like NH, $\Delta N = -1$, $\Delta J = -1$ with $J = N + 1$ gives the strongest lines for to the ground state and first excited state, respectively.

4.3 Comparison between the excitation of NH and ND

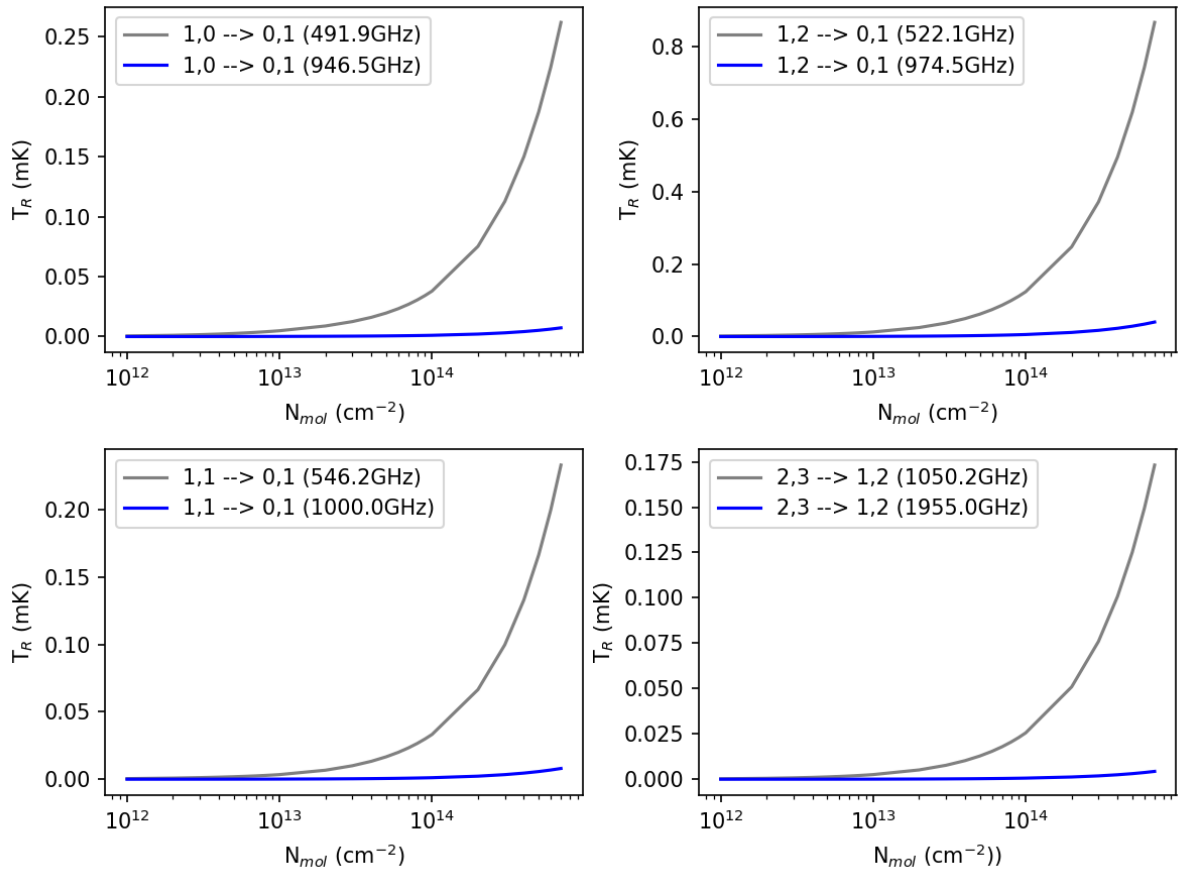

Figure 10: Comparison between the radiation temperature as a functions of column density of the transitions to the ground state and the $2,3 \rightarrow 1,2$ transition of NH (blue) and ND (grey) at $T_{kin} = 30$K and $n(\mathrm{H_2}) = 100$ cm^{-3}.

.

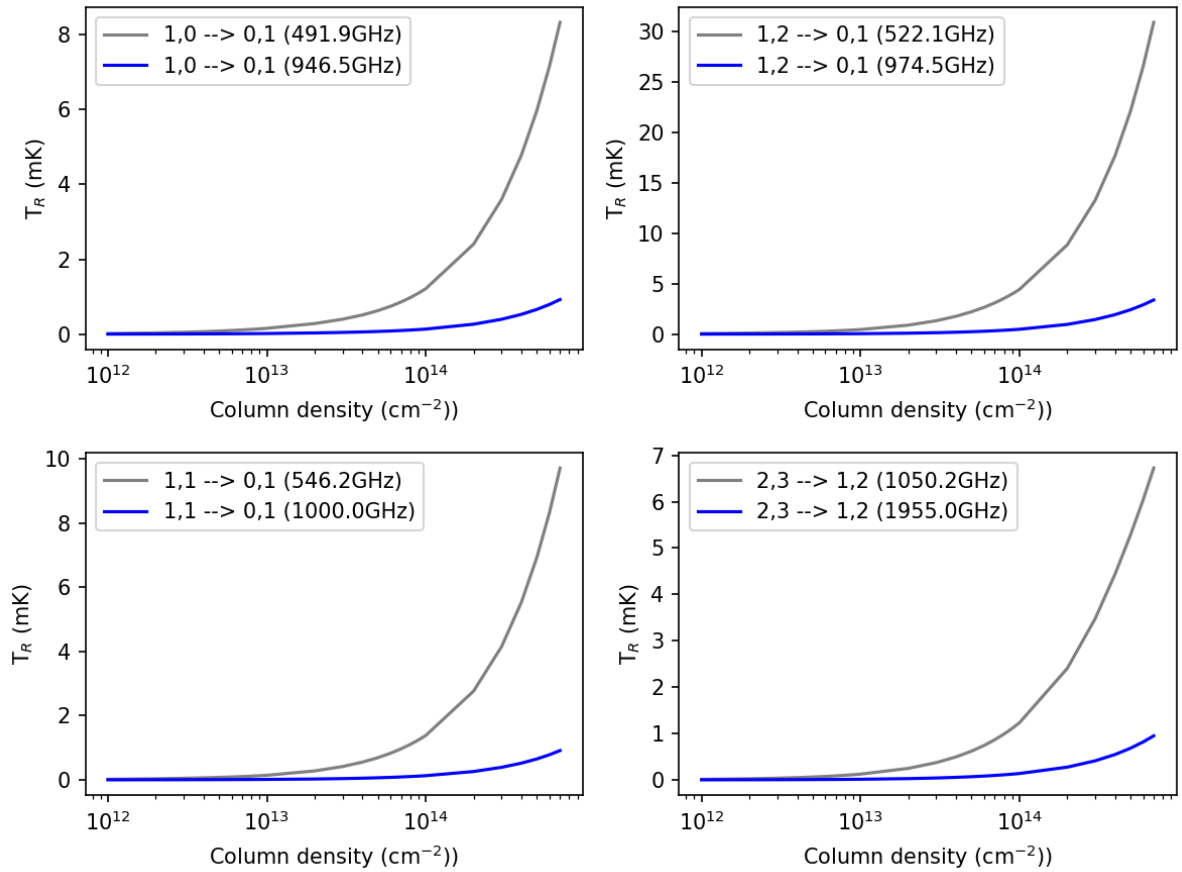

Figure 11: Comparison between the radiation temperature as a functions of column density of the transitions to the ground state and the $2,3 \rightarrow 1,2$ transition of NH (blue) and ND (grey) at $T_{kin} = 100$K and $n(\mathrm{H_2}) = 500$ cm^{-3}.

Figures (10) and (11) clearly underline the difference in excitation between the isotopologues NH and ND. For equal column densities and the same transitions in terms of quantum numbers, the emissions of ND exceed those of NH. If one considers the energy diagram of the two species (3), it is evident that the $N = 1$ triplet, just like all the other triplets, of ND sits at a lower energy than the same triplet for NH. This strictly implies that, for ND, less energy is required for a transition between the first excited state and the ground state to occur, as well as between the higher excited states. Speaking in terms of collisions, ND requires less kinetic energy to enter higher rotational states than NH, thus implying that transitions between the triplets occur at a higher rate for ND, which makes an emission line stronger. Both both extremes, in terms of $\mathrm{H_2}$ density and temperature, of diffuse molecular clouds the difference in excitation is apparent.

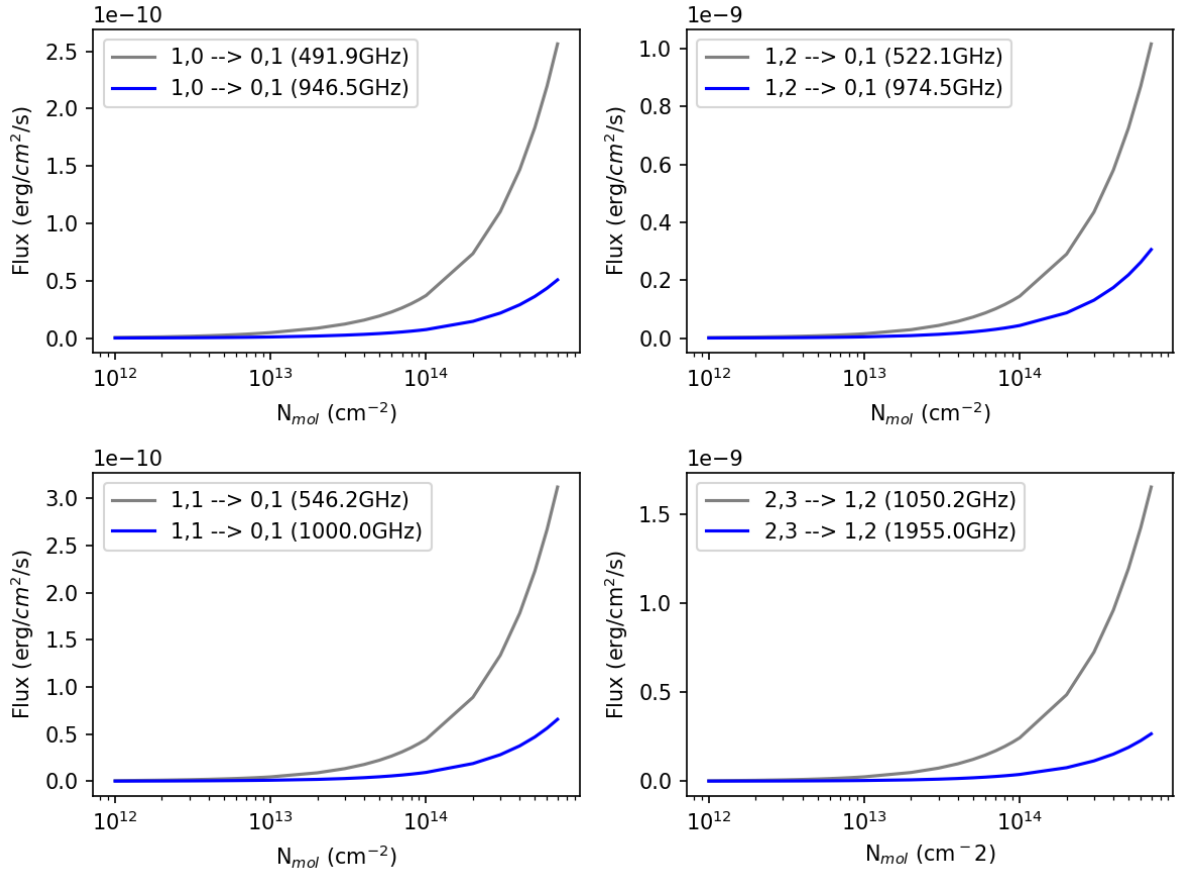

Figure 12: Comparison between the flux as a functions of column density of the transitions to the ground state and the $2,3 \rightarrow 1,2$ transition of NH (blue) and ND (grey) at $T_{kin} = 30$K and $n(\mathrm{H_2}) = 100$ cm^{-3}.

.

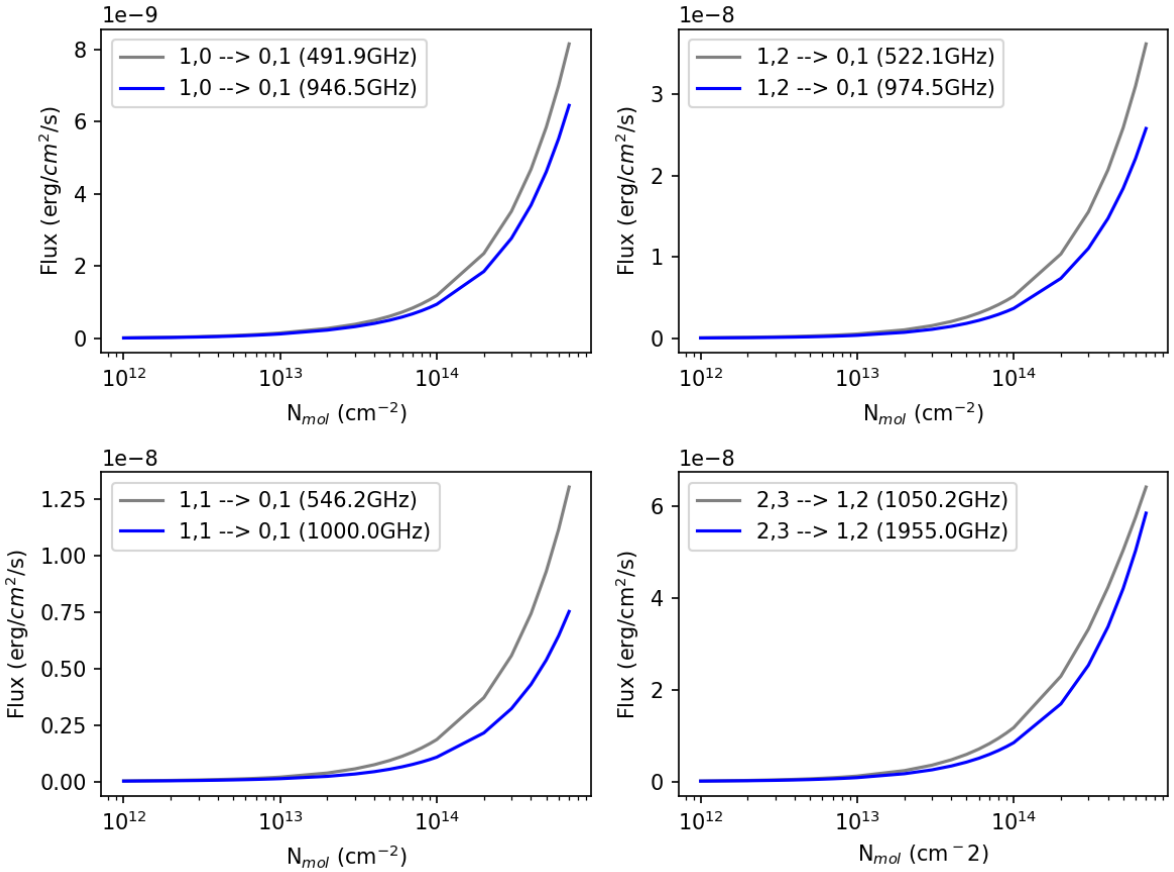

Figure 13: Comparison between the flux as a functions of column density of the transitions to the ground state and the $2,3 \rightarrow 1,2$ transition of NH (blue) and ND (grey) at $T_{kin} = 100$K and $n(\mathrm{H_2}) = 500$ cm^{-3}.

Similarly to the radiation temperature, the flux produced by ND transitions is higher than the one produced by NH transitions. For diffuse clouds of low density and temperature (12), the difference in flux is significant. For diffuse clouds on the high end of density and temperature, the flux of NH emissions approaches that of ND lines. This is indicative of the gaussian line profiles of NH being wider than those of ND, because 10 and 6 show that the peak of the ND profiles are higher.

4.4 Observational Constraints for NH and ND in Diffuse Clouds

Presented below are two tables (4, 5) that show the requirements for NH and ND spectral lines to be detectable. The left-most columns indicate the frequency of the line with the kinetic energy of the cloud being in the column to its right. The right-most column indicates the minimally required molecular column density above which the radiation temperature of the line exceeds 1 mK. To the left of that column is the number density of molecular hydrogen that corresponds to the critical molecular column density along with the kinetic temperature to its left.

Table 4: Constraints for the detection of NH in diffuse molecular clouds

Line	T_{kin} (K)	$n(H_2)$ (cm^{-3})	N_{mol} ($\cdot 10^{14} cm^{-2}$)
946.5 GHz	100	500	7.0
974.5 GHz	75	500	3.6
	100	400	2.5
		500	2.0
1000.0 GHz	100	500	7.0
1955.0 GHz	100	500	7.0

Table 5: Constraints for the detection of ND in diffuse molecular clouds

Line	T_{kin} (K)	$n(H_2)$ (cm^{-3})	N_{mol} ($\cdot 10^{13}$ cm^{-2})
491.9 GHz	100	500	8.1
522.1 GHz	50	500	6.1
	75	200	8.5
		300	5.4
		400	4.2
		500	3.2
	100	200	5.6
		300	3.8
		400	2.7
		500	2.2
546.2 GHz	100	500	8.1
1050.2 GHz	100	500	8.1

4.5 NH and ND in Dark Clouds

4.5.1 Effects of Dust Temperature

As alluded to previously (see section 1.1), dust temperature is a non-negligible factor when performing radiative transfer calculations in dark clouds. Recalling equation (11), the dust temperature should have a dimming effect on the emissions, and pending on how high the dust temperature is, absorption lines may start to take the emission line's place.

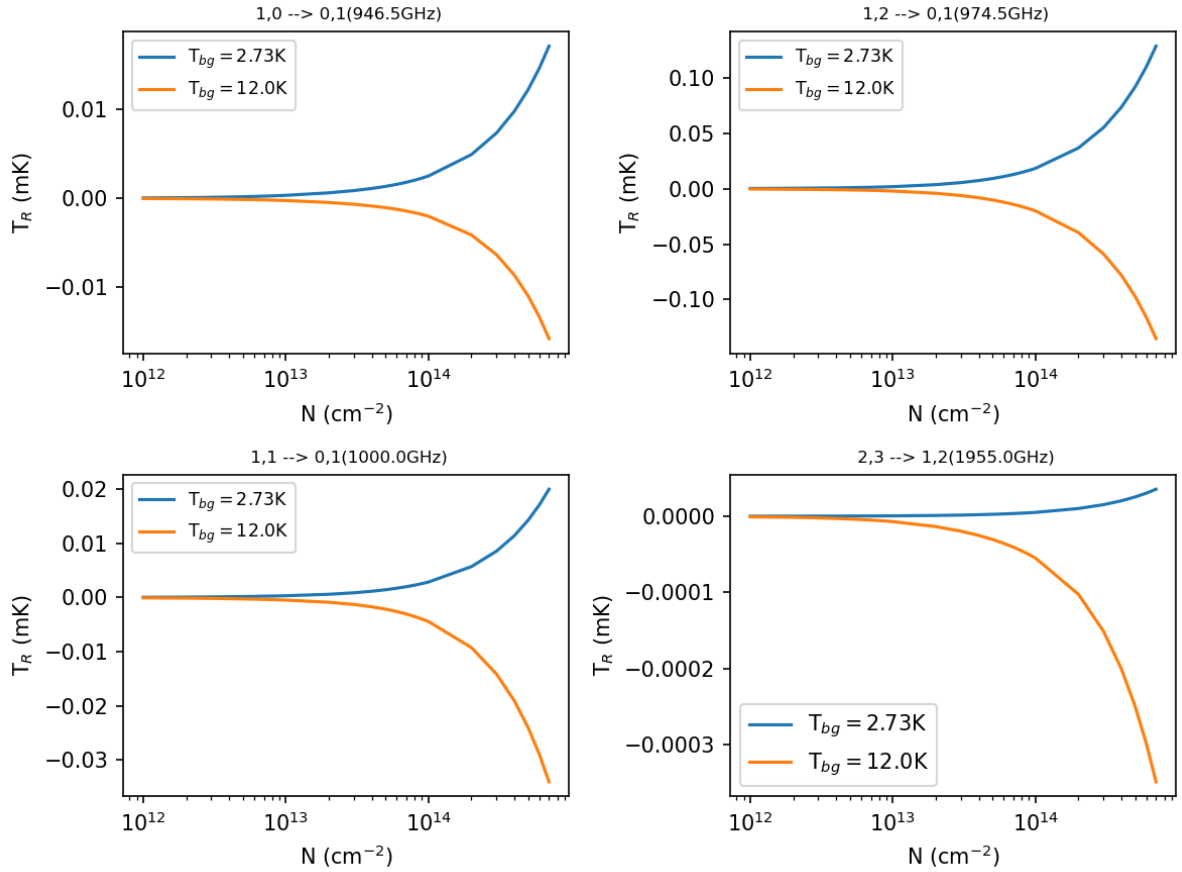

Figure 14: Radiation temperature as a function of column density for the strongest NH lines at a kinetic temperature of 10 K and a molecular hydrogen density of 10^4 cm^{-3}. The CMB (cosmic microwave background) as background temperature is designated by the blue curve, and the dust temperature as background temperature is presented by the orange curve.

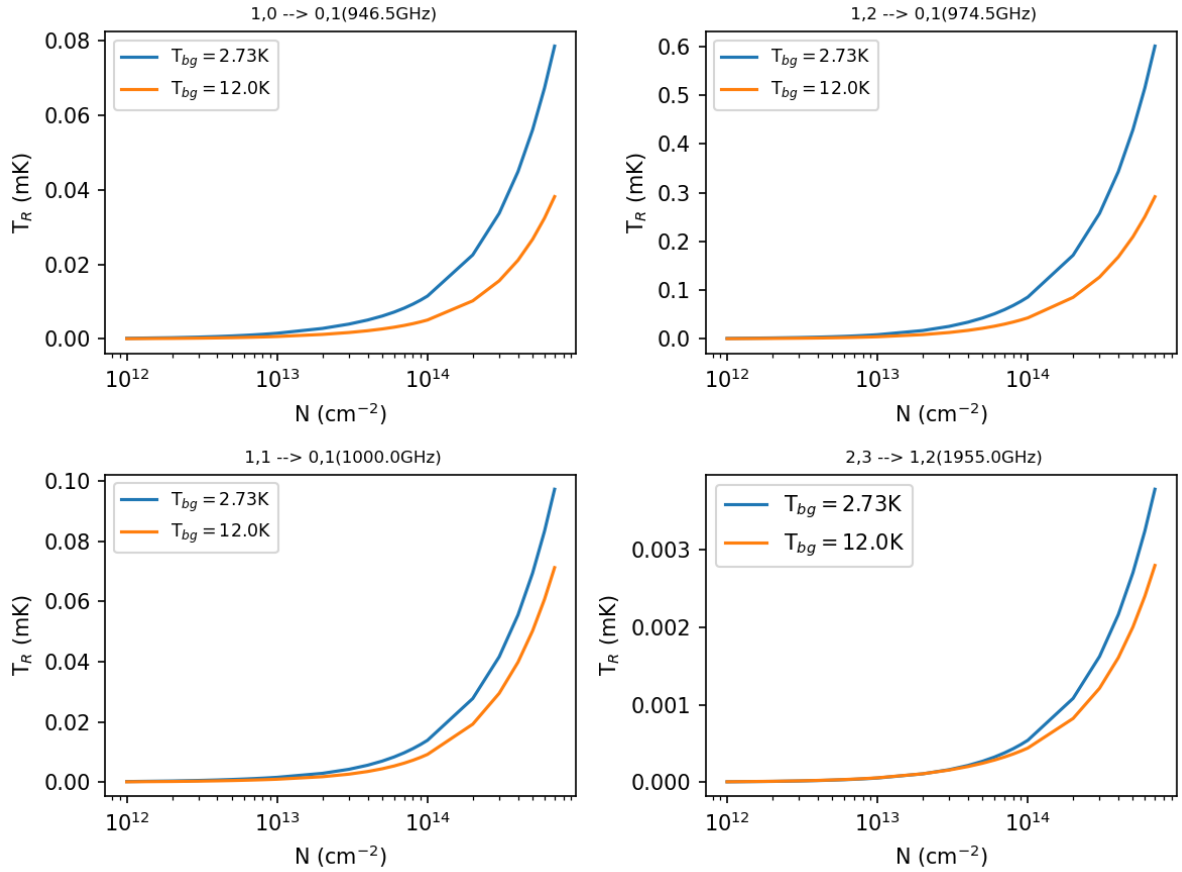

Figure 15: Radiation temperature as a function of column density for the strongest NH lines at a kinetic temperature of 15 K and a molecular hydrogen density of 10^4 cm^{-3}. The CMB (cosmic microwave background) as background temperature is designated by the blue curve, and the dust temperature as background temperature is presented by the orange curve.

Figure (14) shows that for a dust temperature exceeding the kinetic temperature, the emission lines are replaced by absorption lines because the radiation temperature is below zero. Changing the density has no effect on the sign of the radiation temperature. On the other hand, if the kinetic temperature of the gas exceeds the dust temperature, the emission lines remain, but there the lines are attenuated, as demonstrated in figure (15). The same effect is observed for ND lines.

4.5.2 Observational Constraints

Presented below are two tables (6, 7) that show the requirements for NH and ND spectral lines to be detectable in dark clouds.

Table 6: Constraints for the detection of NH in dark clouds at a dust temperature of 12 K.

Line	T_{kin} (K)	$n(H_2)$ (cm^{-3})	N_{mol} (10^{14} cm^{-2})
946.5 GHz	20	$1 \cdot 10^5$	5.1
974.5 GHz	10	$1 \cdot 10^5$	5.0
	15	$5 \cdot 10^4$	4.8
		$1 \cdot 10^5$	2.4
	20	$5 \cdot 10^4$	1.2
		$1 \cdot 10^5$	0.72
1000.0 GHz	20	$1 \cdot 10^5$	3.0
1955.0 GHz	20	$1 \cdot 10^5$	> 10.0

Table 7: Constraints for the detection of ND in dark clouds at a dust temperature of 12 K.

Line	T_{kin} (K)	$n(H_2)$ (cm^{-3})	N_{mol} ($\cdot 10^{13}$ cm^{-2})
491.9 GHz	15	$5 \cdot 10^4$	7.3
		$1 \cdot 10^5$	3.4
	20	$5 \cdot 10^4$	2.1
		$1 \cdot 10^5$	1.1
522.1 GHz	10	$5 \cdot 10^4$	6.1
		$1 \cdot 10^5$	3.0
	15	$5 \cdot 10^4$	2.9
		$1 \cdot 10^5$	1.3
	20	$1 \cdot 10^4$	4.3
		$5 \cdot 10^4$	0.74
		$1 \cdot 10^5$	0.32
546.2 GHz	10	$1 \cdot 10^5$	7.4
	15	$5 \cdot 10^4$	7.1
		$1 \cdot 10^5$	3.6
	20	$5 \cdot 10^4$	2.1
		$1 \cdot 10^5$	1.0
1050.2 GHz	20	$1 \cdot 10^5$	2.6

4.6 Methyl Formate in Dark Clouds

4.6.1 Effects of Temperature and Density

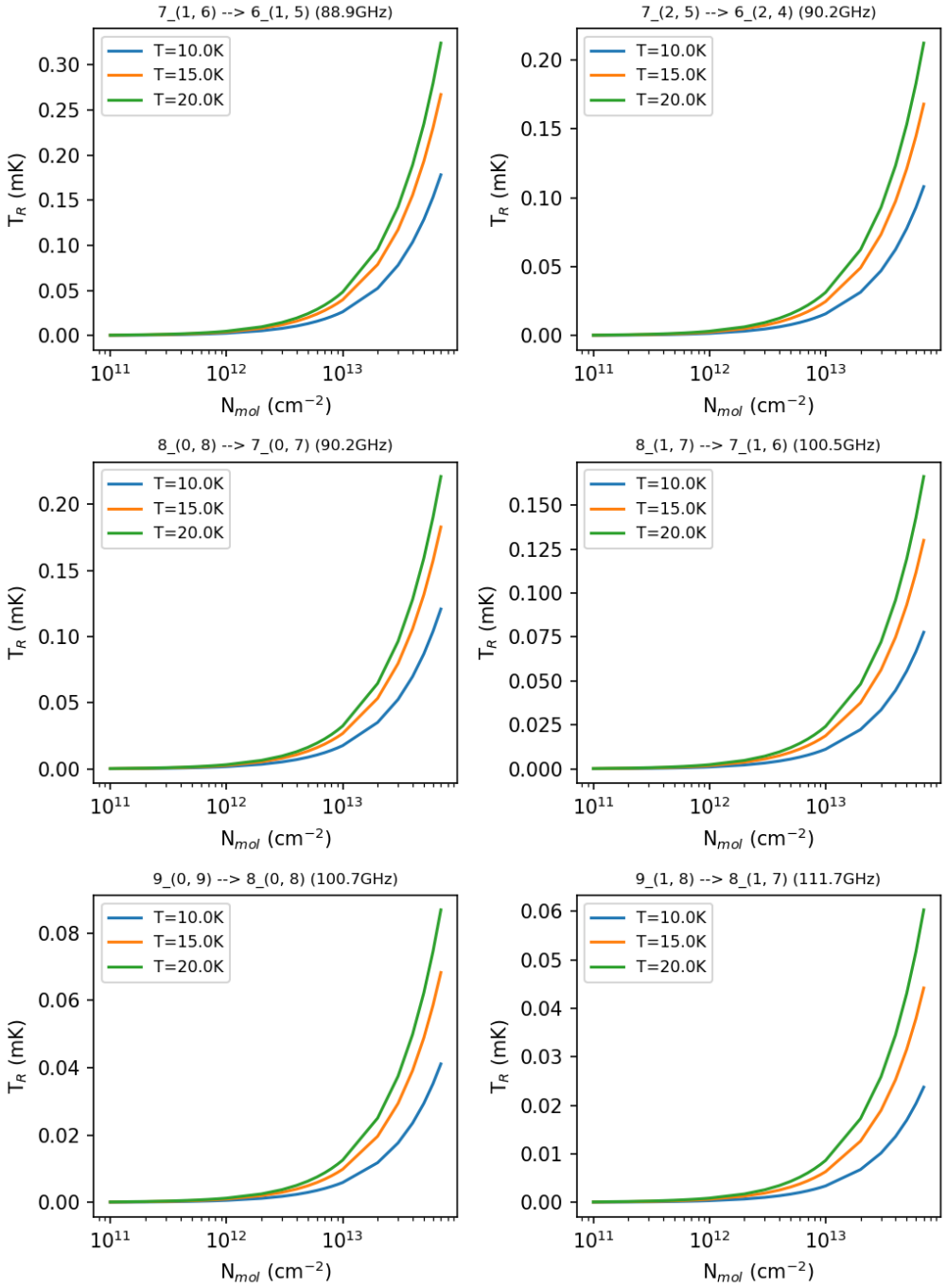

Figure 16: Radiation temperature of the six selected radiative transitions as a function of column density for a fixed H_2 number density of $1 \cdot 10^4$ cm^{-3} and different kinetic temperatures, as indicated by the different colours. The background temperature is that of the CMB.

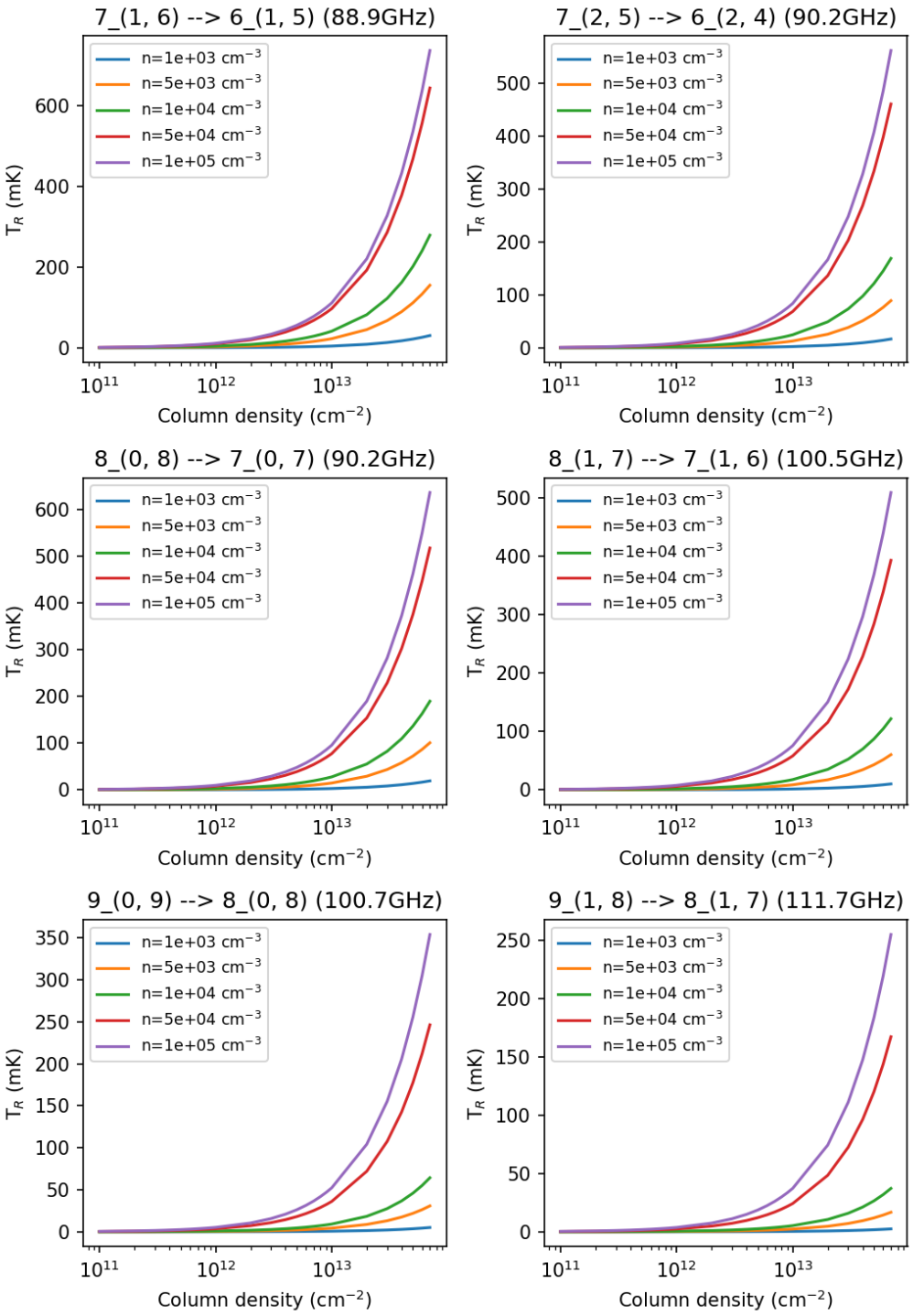

Figure 17: Radiation temperature of the six selected radiative transitions as a function of column density for a fixed kinetic temperature of 10K and different H_2 number densities of $1 \cdot 10^4$ cm^{-3}, as indicated by the different colours. The background temperature is that of the CMB.

As can be observed from figure (16), increasing the kinetic temperature leads to the increase of the line strength for equal molecular column densities. Analogously, by considering figure (17), increasing the molecular hydrogen number density also produces greater line strengths for equal molecular column densities.

4.6.2 Effects of Dust Temperature

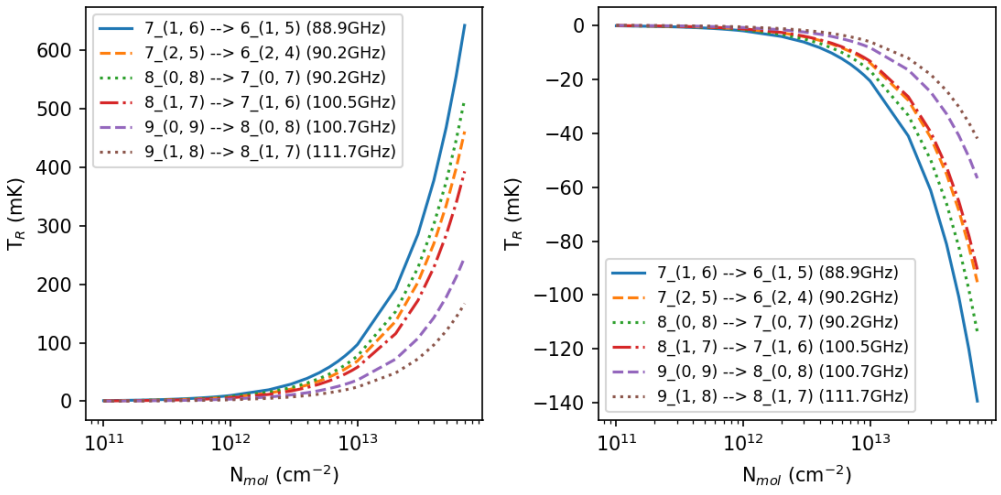

Figure 18: Comparison between the radiation temperature as a function of molecular column density of the six methyl formate transitions, represented by different colours and linestyles, for the CMB background temperature on the left and a dust temperature of 12K on the right. The kinetic temperature sits at 10K and the H_2 number density at $5 \cdot 10^4$ cm^{-3}.

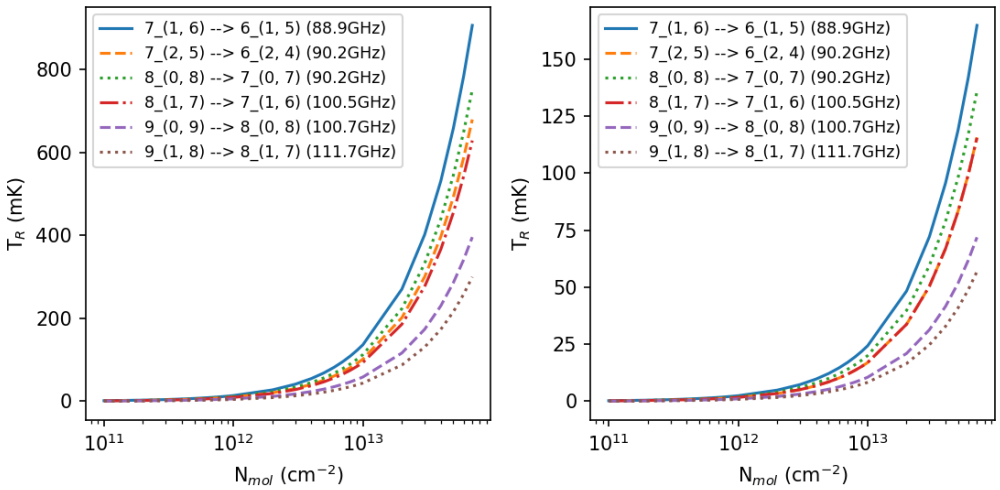

Figure 19: Comparison between the radiation temperature as a function of molecular column density of the six methyl formate transitions, represented by different colours and linestyles, for the CMB background temperature on the left and a dust temperature of 12K on the right. The kinetic temperature sits at 15K and the H_2 number density at $5 \cdot 10^4$ cm^{-3}.

From figure (18), it can be said a dust temperature of 12K induces the emergence of absorption lines in a cloud of a kinetic energy lower than that of the dust, because the line strengths are negative.

Figure (19) shows that if the kinetic temperature of the gas exceeds the dust temperature, emission lines once more emerge. Comparing it to the CMB case, one sees that the radiation field from the dust severely attenuates the line strengths.

4.6.3 Observational constraints

Presented in below are the minimally required molecular column densities in units cm^{-2} for any given set of molecular hydrogen number density $n(H_2)$ and kinetic temperature of the gas T_{kin} at a dust temperature of 8K (table (8)) and 12K (table (9)), respectively. Each table is divided into two parts, as marked by the double vertical line. The left part refers to the group of lines from 88-100.5 GHz whereas the right covers the lines from 100.7-111.7 GHz.

Table 8: Constraints for the detection of methyl formate in cold dark clouds at a dust temperature of $T_{dust} = 8$K.

	T_{kin} (K)					
n(H_2) (cm^{-3})	10	15	20	10	15	20
1e4	$1.9{\cdot}10^{13}$	$6.6{\cdot}10^{12}$	$4.4{\cdot}10^{12}$	$5{\cdot}10^{13}$	$1.6{\cdot}10^{13}$	$1{\cdot}10^{13}$
5e4	$7{\cdot}10^{12}$	$2.1{\cdot}10^{12}$	$1.5{\cdot}10^{12}$	$1.4{\cdot}10^{12}$	$4.4{\cdot}10^{12}$	$3{\cdot}10^{12}$
1e5	$5.1{\cdot}10^{12}$	$1.6{\cdot}10^{12}$	$1.1{\cdot}10^{12}$	$1{\cdot}10^{13}$	$3{\cdot}10^{12}$	$2{\cdot}10^{12}$

Table 9: Constraints for the detection of methyl formate in cold dark clouds at a dust temperature of T_{dust} = 12K.

		T_{kin} (K)					
		10	15	20	10	15	20
$n(H_2)$ (cm^{-3})	1e4	$2.2{\cdot}10^{13}$	$1.7{\cdot}10^{13}$	$7.0{\cdot}10^{12}$	$5.5{\cdot}10^{13}$	$4.3{\cdot}10^{13}$	$1.7{\cdot}10^{13}$
	5e4	$7.4{\cdot}10^{12}$	$5.3{\cdot}10^{12}$	$2.8{\cdot}10^{12}$	$1.6{\cdot}10^{13}$	$1.1{\cdot}10^{13}$	$4.2{\cdot}10^{12}$
	1e5	$5.1{\cdot}10^{12}$	$5.5{\cdot}10^{12}$	$1.2{\cdot}10^{12}$	$1.0{\cdot}10^{13}$	$8.0{\cdot}10^{12}$	$3.4{\cdot}10^{12}$

4.6.4 Comparison to Bacmann et al., 2012

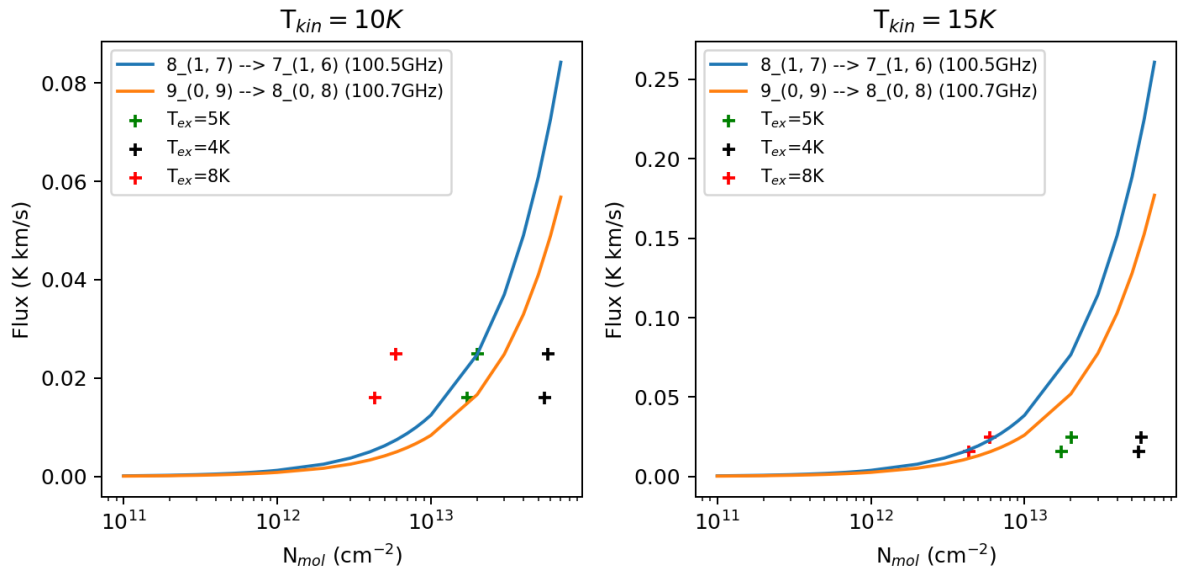

Figure 20: Flux ($K\,km\,s^{-1}$) as a function of molecular column density for the 100.5 (blue curve) GHz and 100.7 GHz (orange curve) lines. The markers refer to the column densities that were inferred by Bacmann et al., 2012 based on the indicated excitation temperatures and the observed line fluxes (0.025 ($K\,km\,s^{-1}$) for the 100.5GHz (top row) and 0.016 $K\,km\,s^{-1}$) for the 100.7GHz (bottom row) line). The physical parameters on the left are T_{dust} = 8K, T_{kin} = 10K, $n(H_2) = 10^5$ cm^{-3}, whereas those for the graph on the right are T_{dust} = 8K, T_{kin} = 15K, $n(H_2) = 10^5$ cm^{-3}.

As can be seen from figure (20), the calculated line fluxes for a dust temperature of 8K and a kinetic temperature of 10K match the column densities found in Bacmann et al., 2012 for an excitation temperature T_{ex} of 5K. Moreover, for a kinetic temperature of 15K, the computed column densities corresponding to Bacmann et al., 2012's observed line fluxes match the column densities for an excitation temperature of 8K of Bacmann.

The excitation temperatures that were found in this study were 8.95K for the 100.5 GHz line and 9.30K for the 100.7 GHz line, at kinetic temperature of 10K, and 12.15K for the 100.5 GHz

line and 10.65K for the 100.7 GHz line, at kinetic temperature of 15K

5 Discussion

5.1 Observation of NH and ND spectral lines in Diffuse Molecular Clouds

Based on the results from section (4.5.2), it may be said that observing NH and ND lines within diffuse molecular clouds with current instruments is an unlikely event to occur. Assuming that the Herschel HIFI instrument can detect down to 1 mK, the only emission line that can hoped to be observed is the 974.5 GHz line. To observe this line requires diffuse clouds to be at the high end in terms of temperature and molecular hydrogen density in addition to NH column densities close to the highest value to have been observed (Hily-Blant et al., 2010). Any lower H_2 density or kinetic temperature than the ones given in table (4) will make this line undetectable for modern instruments. At maximum H_2 density and kinetic temperature, the other NH emission lines require NH column densities above the detected limit, hence making them elusive to modern instruments. The key takeaway from this is that only diffuse molecular clouds at the high end of the temperature and density spectrum are able to produce observable emission lines, with the best candidate being the 974.5 GHz line, according to these calculations.

From table (5), one can infer that similarly to NH, the $1,2 \rightarrow 0,1$ transition , corresponding to the 522.1 GHz line, displays the highest potential for detection. At elevated kinetic temperatures, the required column densities are on the low end of $1 \cdot 10^{13}$ cm^{-2} which are feasible abundances. Higher kinetic temperatures and molecular hydrogen densities are of course more conducive in providing better conditions for observable emission lines (6,7). It is clear that contrary to NH, the necessary conditions for ND do not require near maximum temperatures and densities within the clouds to produce theoretically detectable emission lines.

However, detecting the 974.5 GHz line of NH and 522.1 GHz line of ND within diffuse molecular clouds is an unlikely event to occur. The critical value of 1 mK as the needed line strength for detection is admittedly an optimistic choice of value. It requires background noise to be at an absolute minimum and observing conditions to be optimal. Moreover, as stated in (1.1), diffuse molecular clouds are surrounded by atomic clouds, thus requiring additional extinction factors to be accounted for. This strictly implies that even higher molecular column densities are required for a detection. Additionally, diffuse molecular clouds have a significant fraction of atomic hydrogen, with $n_H/n(\mathrm{H}_2 > 0.1$. This means that the hydrides may also collide with atomic hydrogen, and not solely with molecular hydrogen. For the calculations that were performed, however, only molecular hydrogen was considered as a collision partner. Scaling the He-rate coefficients to H-rate coefficients in the same manner as was done for to obtain the H_2-rate coefficients (by using equation (4)) is not a valid method. Instead, the methods described in section (3.1) must be used.

Coming back to ND, table (5) and figures (10),(11) suggest that observing ND will prove to be a simpler task than observing NH, given that less column density, as well as slightly lower temperatures and H_2 densities are required. However, ND is most probably not very abundant

in clouds with kinetic temperatures that high, let alone diffuse molecular clouds in general. The formation of ND requires deuterated molecular hydrogen, as detailed in section (1.1) . The fractionation processes that contribute to the formation of deuterated molecules is most efficient at lower temperatures, namely at around 10 K. Moreover, the fractional abundance of HD with respect to H_2 is also quite small in diffuse clouds ($10^{-7} - 10^{-6}$ Snow and McCall, 2006), thus making the reservoir for deuterated molecules to form quite depleted to begin with. The kinetic temperatures in diffuse clouds, even at their lowest, are therefore not conducive to the formation of ND, making its fractional abundance with respect to NH probably a lot lower than Gerin et al., 2016's estimate.

Considering NH again, the column densities shown in table (4) are of the order 10^{14}, which is the same as presented in various papers (Hily-Blant et al., 2010,Bacmann et al., 2010,Persson et al., 2012). However, the regions of the ISM that were considered in those papers are far denser regions and not diffuse molecular clouds. In fact, the NH column density within diffuse clouds has been determined to be a lot lower than in dense clouds. Crawford and Williams, 1997, who detected the same NH line as Meyer and Roth, 1991 using spectroscopic absorption in the diffuse cloud towards the star ζ Oph found column densities approaching 10^{12} cm^{-2}. More recently, Weselak et al., 2009 calculated the NH column densities within several diffuse clouds towards different stars and found that all of them figured in the order of 10^{12} cm^{-2}. The presence of stars imply strong radiation fields and therefore elevated background temperatures. To account for this using RADEX, models of radiation fields would have to be made instead of using the CMB background temperature. With this in mind and knowing from table (4) that column densities of the order of 10^{14} cm^{-2} are required to allow the detection of collisionally induced emission lines, it thus follows that NH in diffuse molecular clouds can't be detected with modern instruments. The line strengths at lower column densities in diffuse clouds are just too low for NH (in the range of $10^{-6} - 10^{-7}$ K).

5.2 Observation of NH and ND spectral lines in Dark Clouds

Looking at table (6), it becomes apparent that just like it is the case for diffuse clouds, the 974.5 GHz line once more displays the highest line strengths for equal conditions and molecular column densities out of all emission lines. It was found that in order to obtain a detectable rotational absorption line for NH at a dust temperature of 12K requires the cloud to be very dense and a NH column density of $5.1 \cdot 10^{14}$ cm^{-2}, so above the thus far highest detected NH column density. At a kinetic temperature of 15K and molecular hydrogen density of $1 \cdot 10^5$ cm^{-3} a radiation temperature of 1 mK is reached at $2.4 \cdot 10^{14}$ cm^{-2}. At $T_{kin} = 20$K, a less dense cloud will suffice to obtain detectable emissions at a column density of $2.3 \cdot 10^{14}$ cm^{-2}. For a the densest dark clouds (not shown), the minimum column density stands at $7 \cdot 10^{13}$ cm^{-2}. The 1000 GHz line also stands a chance of being detectable, namely when both density and kinetic temperature are at their highest, and NH has a column density of $3 \cdot 10^{14}$ cm^{-2}.

Looking at table 7, it becomes evident that contrary to ND in diffuse clouds, transitions other

than solely the 522.1 GHz are theoretically observable. On the absorption side, both the 522.1 GHz and the 546.2 GHz reach radiation temperatures of -1 mK at ND column densities of the order 10^{13} cm^{-2}. The most conducive conditions for strong emission lines occur at a kinetic temperature of 20K and in very dense dark clouds. Almost all the ground state transitions, as well as the $3,2 \rightarrow 1,2$ transition, require ND column densities just above 10^{13} cm^{-2}. The 522.1 GHz reaches the critical radiation temperature at column densities below 10^{13} cm^{-2}.

Observing NH and ND in dark clouds is far more feasible than it is for diffuse clouds. The minimum required column densities that were found with the calculations are of the same order of magnitude as those determined in papers that considered the two isotopologues in these regions (Bacmann et al., 2010,Persson et al., 2010, Hily-Blant et al., 2010). However, it has to be said that comparing these results to those studies is quite difficult, given that the observations were that of NH or ND absorption lines toward the protostar IRAS 16293-2422 and the protostellar region G10.6-0.4. Additionally, calculations that they made featured models of radiation fields, which wasn't done for this study.

Considering table (7), one would be inclined to say that higher temperatures and densities are the most conducive to observe ND spectral lines. However, the same arguments apply here as they did for ND in diffuse clouds. The formation of ND occurs ideally at 10 K, meaning that its abundance in slightly warmer clouds is reduced.

5.3 NH and ND abundance fractions

The total elemental abundance of nitrogen nuclei in diffuse molecular clouds may assumed to be around $n_N/n_H = (6.5 - 7.2) \cdot 10^{-5}$ (Gerin et al., 2016, Le Gal et al., 2014, Maciel, 2015). The atomic form of nitrogen is generally speaking much more abundant than molecular nitrogen and other nitrogen-bearing molecules, though this is medium-dependent, one may safely assume that $n(\mathrm{N})/n_{\mathrm{N}} \simeq 1$, where n_{N} refers to the total number density of nitrogen, including molecular species.

Since dark clouds provide better grounds for the detection of NH and ND emissions, they also provide better opportunities to estimate abundances through observation. The column density of hydrogen in dark clouds is said to figure around $N_{\mathrm{H}} = 10^{23}$ cm^{-2}. To observe NH requires it to have column densities of the order of $N(\mathrm{NH}) = 1 \cdot 10^{14}$ cm^{-2} (see table (6)). This enables the calculation of the ratio of abundances between NH and H_2, which turns out to be of the order of 10^{-9}. With this, one can find an estimate of the fraction of nitrogen that is contained within the imidogen radical in dark clouds:

$$\frac{n(\mathrm{NH})}{n_{\mathrm{N}}} \simeq 1.4 \cdot 10^{-5} - 1.5 \cdot 10^{-4} \tag{18}$$

The value obtained in equation (18) is, as stated an estimate. However, the method of deriving it mustn't be underscored. Now that collision data for both NH and ND is available to perform non-

LTE radiative transfer calculations to obtain molecular line strengths, it is possible to directly infer abundances based on observed line strengths and knowledge of the physical parameters of the observed medium.

Considering ND, the ratio of its abundance with respect to NH is still very much a topic of debate. The abundance ratios of Gerin et al., 2016 and Bacmann et al., 2010 are still shrouded with uncertainty because first of all, the excitation of ND is contrasts significantly to NH. This is demonstrated with figures (10, 11, 12 and 13). ND, due to its lower rotational constants, has rotational levels that are much more thinly spaced than NH, meaning that less energy is required to excite ND to higher levels. Refining knowledge about the ND/NH fraction is crucial. If constrained, it becomes possible to directly infer the abundance of one isotopologue based on knowledge of the other's abundance. This would allow chemical models to be refined as well, considering that the fractionation processes of deuterated molecules aren't entirely understood

5.4 Observing Methyl Formate in Dark Clouds

Based on the results presented in tables (8) and (9), it can be said that dark clouds present promising grounds for the detection of methyl formate spectral lines resulting from collisions with H_2. The molecular column densities that were determined to produce line strengths of at least 10 mK fall well into the range of expected abundances within these environments. Fractional abundance with respect to molecular hydrogen of methyl formate in dark clouds figures at $10^{-11} - 10^{-10}$ (Faure et al., 2014). Molecular hydrogen column densities stand at around 10^{23} cm^{-2} in dark clouds, thus yielding methyl formate column densities in the range that was determined here as minimum requirements to produce observable spectral lines. The most conducive conditions for spectral lines were found to be when the dust temperature is at its lowest, and kinetic energy at its highest. This makes intuitive sense, given that the lower the dust temperature, the lower the attenuation effect.

One of the main reasons why methyl formate should be relatively easy to detect lies within the fact that its rotational levels aren't very high in energy. The first 65 rotational levels, in fact, all have energies less than 20 cm^{-1}. Moreover, the levels are generally speaking very thinly spaced. This means that relatively little kinetic energy, which translates to lower kinetic temperatures, suffices for the ester to enter excited rotational states as a result of collisions with H_2. Additionally, given that methyl formate is comprised of 8 atoms, it is a fairly large molecules with respect to most interstellar molecules, which translates to a larger collision cross section. This makes the rate coefficients to be larger in magnitude as well. However, it must once again be emphasized that results that were obtained aren't necessarily accurate on the grounds of the scaling of the rate coefficients (van der Tak et al., 2020).

5.5 Comparison to Bacmann et al., 2012

Bacmann et al., 2012 observed the prestellar core L1689B, which is characterized by dust temperatures of $11-12$K, a central density figuring at 10^5 cm^{-3} and a gas temperature of $7-10$ K. In the conduct of this study, it was found that for a dust temperature of 8K and a gas temperature of 10K, as well as a gas temperature of 15K, the emission line fluxes were reproduced for similar molecular column densities, as can be seen in figure (20).

Reproducing the physical conditions of L1689B, and taking the dust temperature as the background temperature, within RADEX, lead to the formation of absorption lines because the background temperature exceeded the kinetic temperature. This shows that simply taking the dust temperature as the background temperature doesn't necessarily produce accurate results. The dust radiation would therefore better be accounted for by the inclusion of a radiation field produced by dust emissions in RADEX's calculations.

The difference in methods that were used is clear cut. Bacmann et al., 2012 used the observed line fluxes and an estimate of the excitation temperature to fit Gaussians to the emission lines using the CLASS routine[11]. Here, the physical conditions were simulated in a the non-LTE radiative transfer code RADEX, which takes both radiative and collision processes into account. Then, the column densities corresponding to the line fluxes were selected.

The excitation temperatures that were found in this study exceed those determined by Bacmann et al., 2012. Using equation (6), one sees that the higher the excitation temperature, the more substantial the population of a higher energy level is. This means that according to the calculations performed with RADEX, the $8_{1,7}$ and $9_{0,9}$ levels are more populated than what Bacmann et al., 2012 found. This may be due to the higher kinetic temperatures used in the calculations, meaning that the molecules had higher kinetic energies and thus could more easily enter higher excited states.

[11] https://www.iram.fr/IRAMFR/GILDAS/

6 Conclusions and Outlook

To summarize, it was found that observing collisionally-induced emissions of NH and ND in diffuse molecular clouds is highly unlikely. The required column densities for the two species for regions without a strong radiation field exceed those of observed column densities within diffuse clouds. On the other hand, detecting the two hydrides in dark clouds is more probable. Both isotopologues are more abundant in these regions, especially ND because its formation is most efficient at temperatures of 10K. However, modern instruments will probably not suffice to guarantee a detection. For this, future telescopes capable of detecting molecular emissions of line strengths standing at fractions of 1mK will most likely be needed.

Dark clouds provide good conditions for the observation of methyl formate spectral lines. The deduced column densities that are necessary to produce detectable lines fall within the range of expected abundances of the organic compound.

Limitations that apply to his study are first of all the fact that the rate coefficients were all scaled from He system to H_2 systems. In the case of diffuse clouds, the fraction of atomic hydrogen isn't negligible, thus calling for collision rate coefficients to be computed for NH-H and ND-H systems. Additionally, no radiation fields were modelled for the calculations performed with RADEX, making it difficult to draw comparisons with other studies. Diffuse clouds are mostly quite close to stars, and dark clouds to protostars in addition to being permeated by dust emissions.

The relevance of this study mustn't be understated. The construction of data files unifying both spectroscopic and collision data for the molecules NH, ND and CH_3OCHO has enabled the prediction of spectral line intensities and fluxes based on the abundances of the species and the physical conditions of their environment. This means that for any observed molecular line intensity, an immediate estimate of the molecule's abundance can be made provided the physical parameters of the environment are known. With the data files being added to the LAMDA database, this allows other researchers to make their own calculations and predictions and draw comparisons to observations. Of particular interest and necessity to investigate is the abundance ratio of NH and ND. Further research, with the help of the data files, will allow the abundance of one isotopologue to be derived from another. Additionally, narrowing down the uncertainty of the NH/ND ratio will give clear and concise constraints on chemical models accounting for the formation of bot species. A similar thing can also be said for methyl formate. The observation of collisionally-induced spectral lines will shed light unto the formation mechanisms of methyl formate and the rates at which they occur in cold clouds. Presently, the collision data for methyl formate only accounts for temperatures up to 30 K, so calculations are for the moment limited in scope. If higher temperatures are added, then calculations can also be performed for methyl formate in hot cores and corinos.

7 Acknowledgements

It doesn't go without saying that there a number of people that I would like to thank from the bottom of my heart. I therefore give my upmost gratitude to my supervisor, Prof. dr. Floris van der Tak, for providing such a fantastically interesting project, as well as guidance and answers whenever I required them. I also want to thank my former physics teacher from secondary school, Mr Gauthier, who sparked my affinity for the world of physics and without whom I surely wouldn't have made the choice of studying astronomy in Groningen. Of course, I am ever so grateful to my parents, Michèle and Robert, whose unceasing support and belief in me has made me achieve so much and without whom I wouldn't be where I am now. Last but not least, a big thank you also goes out those close to me, be they friends or family, who make life just that much better.

References

Bacmann, A., Caux, E., Hily-Blant, P., Parise, B., Pagani, L., Bottinelli, S., Maret, S., Vastel, C., Ceccarelli, C., Cernicharo, J., Henning, T., Castets, A., Coutens, A., Bergin, E. A., Blake, G. A., Crimier, N., Demyk, K., Dominik, C., Gerin, M., ... Ravera, L. (2010). First detection of ND in the solar-mass protostar IRAS16293-2422 [Publisher: EDP Sciences]. *Astronomy & Astrophysics*, *521*, L42. https://doi.org/10.1051/0004-6361/201015102

Bacmann, A., Taquet, V., Faure, A., Kahane, C., & Ceccarelli, C. (2012). Detection of complex organic molecules in a prestellar core: A new challenge for astrochemical models. *Astronomy & Astrophysics*, *541*, L12. https://doi.org/10.1051/0004-6361/201219207

Bergin, E. A., & Tafalla, M. (2007). Cold Dark Clouds: The Initial Conditions for Star Formation [arXiv:0705.3765 [astro-ph]]. *Annual Review of Astronomy and Astrophysics*, *45*(1), 339–396. https://doi.org/10.1146/annurev.astro.45.071206.100404

Brown, R. D., Crofts, J. G., Godfrey, P. D., Gardner, F. F., Robinson, B. J., & Whiteoak, J. B. (1975). Discovery of interstellar methyl formate. *The Astrophysical Journal*, *197*, L29. https://doi.org/10.1086/181769

Ceccarelli, C. (2008). Organic molecules in protostellar environments. *Proceedings of the International Astronomical Union*, *4*(S251), 79–88. https://doi.org/10.1017/S174392130802125X

Crawford, I. A., & Williams, D. A. (1997). Detection of interstellar NH towards Ophiuchi by means of ultra-high-resolution spectroscopy. *Monthly Notices of the Royal Astronomical Society*, *291*(3), L53–L56. https://doi.org/10.1093/mnras/291.3.L53

Draine, B. (2011). *Physics of the Interstellar and Intergalactic Medium*. Princeton University Press. https://books.google.nl/books?id=XWOYDwAAQBAJ

Dumouchel, F., Klos, J., Toboła, R., Bacmann, A., Maret, S., Hily-Blant, P., Faure, A., & Lique, F. (2012). Fine and hyperfine excitation of NH and ND by He: On the importance of calculating rate coefficients of isotopologues. *The Journal of Chemical Physics*, *137*, 114306. https://doi.org/10.1063/1.4753423

Faure, A., Remijan, A. J., Szalewicz, K., & Wiesenfeld, L. (2014). Weak maser emission of methyl formate toward Sagittarius B2(N) in the Green Bank Telescope PRIMOS Survey [arXiv:1401.1136 [astro-ph]]. *The Astrophysical Journal*, *783*(2), 72. https://doi.org/10.1088/0004-637X/783/2/72

Faure, A., Szalewicz, K., & Wiesenfeld, L. (2011). Potential energy surface and rotational cross sections for methyl formate colliding with helium. *The Journal of Chemical Physics*, *135*(2), 024301. https://doi.org/10.1063/1.3607966

Garrod, R. T., & Herbst, E. (2006). Formation of methyl formate and other organic species in the warm-up phase of hot molecular cores. *Astronomy & Astrophysics*, *457*(3), 927–936. https://doi.org/10.1051/0004-6361:20065560

Garrod, R. T., Weaver, S. L. W., & Herbst, E. (2008). Complex Chemistry in Star-forming Regions: An Expanded Gas-Grain Warm-up Chemical Model. *The Astrophysical Journal*, *682*(1), 283–302. https://doi.org/10.1086/588035

Gerin, M., Neufeld, D. A., & Goicoechea, J. R. (2016). Interstellar Hydrides [arXiv:1601.02985 [astro-ph]]. *Annual Review of Astronomy and Astrophysics*, *54*(1), 181–225. https://doi.org/10.1146/annurev-astro-081915-023409

Gordy, W., & Cook, R. L. (1984). 4.2.3 Molecules in 3 States. In *Microwave Molecular Spectra (3rd Edition)* (pp. 99–108). Knovel. https://app.knovel.com/hotlink/pdf/id:kt003W9YM9/microwave-molecular-spectra/molecules-in-3-sigma

Herbst, E., & Van Dishoeck, E. F. (2009). Complex Organic Interstellar Molecules. *Annual Review of Astronomy and Astrophysics*, *47*(1), 427–480. https://doi.org/10.1146/annurev-astro-082708-101654

Hily-Blant, P., Maret, S., Bacmann, A., Bottinelli, S., Parise, B., Caux, E., Faure, A., Bergin, E. A., Blake, G. A., Castets, A., Ceccarelli, C., Cernicharo, J., Coutens, A., Crimier, N., Demyk, K., Dominik, C., Gerin, M., Hennebelle, P., Henning, T., … Yorke, H. (2010). Nitrogen hydrides in the cold envelope of IRAS 16293-2422. *Astronomy and Astrophysics*, *521*, L52. https://doi.org/10.1051/0004-6361/201015253

Hollis, J. M., Lovas, F. J., & Jewell, P. R. (2000). Interstellar Glycolaldehyde: The First Sugar. *The Astrophysical Journal*, *540*(2), L107–L110. https://doi.org/10.1086/312881

Kroto, H. (1992). *Molecular Rotation Spectra* (Dover Edition) [1. Molecular spectroscopy 2.Molecular rotation]. Dover Publications, Inc. New York.

Le Gal, R., Hily-Blant, P., Faure, A., Forêts, G. P. d., Rist, C., & Maret, S. (2014). Interstellar chemistry of nitrogen hydrides in dark clouds [arXiv:1311.5313 [astro-ph]]. *Astronomy & Astrophysics*, *562*, A83. https://doi.org/10.1051/0004-6361/201322386

Maciel, W. (2015). *Astrophysics of the Interstellar Medium*. Springer New York. https://books.google.nl/books?id=eZrssgEACAAJ

Melosso, M., Bizzocchi, L., Tamassia, F., Esposti, C. D., Canè, E., & Dore, L. (2019). The rotational spectrum of ^{15}ND. Isotopic-independent Dunham-type analysis of the imidogen radical [arXiv:1811.02370 [astro-ph]]. *Physical Chemistry Chemical Physics*, *21*(7), 3564–3573. https://doi.org/10.1039/C8CP04498H

Meyer, D. M., & Roth, K. C. (1991). Discovery of interstellar NH. *The Astrophysical Journal*, *376*, L49. https://doi.org/10.1086/186100

Neill, J. L., Muckle, M. T., Zaleski, D. P., Steber, A. L., Pate, B. H., Lattanzi, V., Spezzano, S., McCarthy, M. C., & Remijan, A. J. (2012). LABORATORY AND TENTATIVE INTERSTELLAR DETECTION OF TRANS-METHYL FORMATE USING THE PUBLICLY AVAILABLE GREEN BANK TELESCOPE PRIMOS SURVEY. *The Astrophysical Journal*, *755*(2), 153. https://doi.org/10.1088/0004-637X/755/2/153

Osterbrock, D., & Ferland, G. (2006). *Astrophysics Of Gas Nebulae and Active Galactic Nuclei*. University Science Books. https://books.google.nl/books?id=6GIXMFpET4cC

Persson, C. M., Black, J. H., Cernicharo, J., Goicoechea, J. R., Hassel, G. E., Herbst, E., Gerin, M., De Luca, M., Bell, T. A., Coutens, A., Falgarone, E., Goldsmith, P. F., Gupta, H., Kaźmierczak, M., Lis, D. C., Mookerjea, B., Neufeld, D. A., Pearson, J., Phillips, T. G., … Planesas, P. (2010). Nitrogen hydrides in interstellar gas: *Herschel* /HIFI

observations towards G10.6-0.4 (W31C). *Astronomy and Astrophysics*, *521*, L45. https://doi.org/10.1051/0004-6361/201015105

Persson, C. M., De Luca, M., Mookerjea, B., Olofsson, A. O. H., Black, J. H., Gerin, M., Herbst, E., Bell, T. A., Coutens, A., Godard, B., Goicoechea, J. R., Hassel, G. E., Hily-Blant, P., Menten, K. M., Müller, H. S. P., Pearson, J. C., & Yu, S. (2012). Nitrogen hydrides in interstellar gas: II. Analysis of *Herschel* /HIFI observations towards W49N and G10.6 0.4 (W31C). *Astronomy & Astrophysics*, *543*, A145. https://doi.org/10.1051/0004-6361/201118686

Prasad, S. S., & Huntress, W. T., Jr. (1980). A model for gas phase chemistry in interstellar clouds. I - The basic model, library of chemical reactions, and chemistry among C, N, and O compounds. *The Astrophysical Journal Supplement Series*, *43*, 1. https://doi.org/10.1086/190665

PubChem. (n.d.). Electronegativity | Periodic Table of Elements. Retrieved June 2, 2023, from https://pubchem.ncbi.nlm.nih.gov/periodic-table/electronegativity

Reutemann, W., & Kieczka, H. (2000). Formic Acid [ISSN: 1435-6007 _eprint: https://onlinelibrary.wiley.com/do In *Ullmann's Encyclopedia of Industrial Chemistry*. John Wiley & Sons, Ltd. https://doi.org/10.1002/14356007.a12_013

Roueff, E., & Lique, F. (2013). Molecular Excitation in the Interstellar Medium: Recent Advances in Collisional, Radiative, and Chemical Processes [ADS Bibcode: 2013ChRv..113.8906R]. *Chemical Reviews*, *113*, 8906–8938. https://doi.org/10.1021/cr400145a

Schoeier, F. L., van der Tak, F. F. S., van Dishoeck, E. F., & Black, J. H. (2005). An atomic and molecular database for analysis of submillimetre line observations [arXiv:astro-ph/0411110]. *Astronomy & Astrophysics*, *432*(1), 369–379. https://doi.org/10.1051/0004-6361:20041729

Sewiło, M., Indebetouw, R., Charnley, S. B., Zahorecz, S., Oliveira, J. M., Van Loon, J. T., Ward, J. L., Chen, C.-H. R., Wiseman, J., Fukui, Y., Kawamura, A., Meixner, M., Onishi, T., & Schilke, P. (2018). The Detection of Hot Cores and Complex Organic Molecules in the Large Magellanic Cloud. *The Astrophysical Journal*, *853*(2), L19. https://doi.org/10.3847/2041-8213/aaa079

Snow, T. P., & McCall, B. J. (2006). Diffuse Atomic and Molecular Clouds. *Annual Review of Astronomy and Astrophysics*, *44*(1), 367–414. https://doi.org/10.1146/annurev.astro.43.072103.150624

Takano, S., Klaus, T., & Winnewisser, G. (1998). The ND Radical: Laboratory Measurement of theN= 2–1 Rotational Transition at 1 THz. *Journal of Molecular Spectroscopy*, *192*(2), 309–319. https://doi.org/10.1006/jmsp.1998.7671

Toboła, R., Dumouchel, F., Kłos, J., & Lique, F. (2011). Calculations of fine-structure resolved collisional rate coefficients for the NH(X3 -)-He system. *J. Chem. Phys.*

van der Tak, Black, J., Schoeier, F., Jansen, D., & van Dishoeck, E. (2007). A computer program for fast non-LTE analysis of interstellar line spectra [arXiv:0704.0155 [astro-ph]]. *Astronomy & Astrophysics*, *468*(2), 627–635. https://doi.org/10.1051/0004-6361:20066820

van der Tak, Lique, F., Faure, A., Black, J. H., & van Dishoeck, E. F. (2020). The Leiden Atomic and Molecular Database (LAMDA): Current Status, Recent Updates, and Future Plans [ADS Bibcode: 2020Atoms...8...15V]. *Atoms*, *8*, 15. https://doi.org/10.3390/atoms8020015

Vasyunin, A. I., & Herbst, E. (2013). REACTIVE DESORPTION AND RADIATIVE ASSOCIATION AS POSSIBLE DRIVERS OF COMPLEX MOLECULE FORMATION IN THE COLD INTERSTELLAR MEDIUM. *The Astrophysical Journal*, *769*(1), 34. https://doi.org/10.1088/0004-637X/769/1/34

Vigren, E., Zhaunerchyk, V., Hamberg, M., Kaminska, M., Semaniak, J., Af Ugglas, M., Larsson, M., Thomas, R. D., & Geppert, W. D. (2012). REASSESSMENT OF THE DISSOCIATIVE RECOMBINATION OF N_2H^+ AT CRYRING. *The Astrophysical Journal*, *757*(1), 34. https://doi.org/10.1088/0004-637X/757/1/34

Weiß, A., Requena-Torres, M. A., Güsten, R., García-Burillo, S., Harris, A. I., Israel, F. P., Klein, T., Kramer, C., Lord, S., Martin-Pintado, J., Röllig, M., Stutzki, J., Szczerba, R., Van Der Werf, P. P., Philipp-May, S., Yorke, H., Akyilmaz, M., Gal, C., Higgins, R., ... Wunsch, H. J. (2010). HIFI spectroscopy of low-level water transitions in M 82. *Astronomy and Astrophysics*, *521*, L1. https://doi.org/10.1051/0004-6361/201015078

Weselak, T., Galazutdinov, G. A., Beletsky, Y., & Kreowski, J. (2009). Interstellar NH molecule in translucent sightlines. *Monthly Notices of the Royal Astronomical Society*, *400*(1), 392–397. https://doi.org/10.1111/j.1365-2966.2009.15466.x